THE UNIVERSITY OF CHICAGO

# NO HURST FOR THE WEARY: SUPPRESSION OF SCALE-FREE BRAIN ACTIVITY AS A MEASURE OF COGNITIVE EFFORT AND PREDICTOR OF WORKING MEMORY PERFORMANCE

A DISSERTATION SUBMITTED TO
THE FACULTY OF THE DIVISION OF THE SOCIAL SCIENCES
IN CANDIDACY FOR THE DEGREE OF
DOCTOR OF PHILOSOPHY

DEPARTMENT OF PSYCHOLOGY

BY

OMID KARDAN

CHICAGO, ILLINOIS

AUGUST 2019

## DEDICATION

I would like to dedicate this work to my father, because he would've enjoyed hearing about this research, and to Marc, for all the time and energy he's dedicated to me.

## TABLE OF CONTENTS

LIST OF FIGURES

LIST OF TABLES

**ACKNOWLEDGMENTS**

I thank my dissertation committee, Dr.'s Marc Berman, Monica Rosenberg, Edward Vogel, and Stephanie Palmer for their insightful feedback and helpful comments.

I thank Kirsten Adam, Nathan Churchill, Irida Mance, Elliot Layden, Kyoung whan Choe, and Muxuan Lyu for help with data acquisition and analysis in chapters 1 and 2.

I thank the Environmental Neuroscience Lab for putting up with my jokes.

I thank Kate Schertz for emotional and grammatical support.

I thank my family for putting up with me for 29 years.

**Abstract**

Since its proposition about 2 decades ago, the theory of assessing the brain as a neural network with self-organized criticality has triggered a multitude of research due to its conceptual appeal. Scale-free brain activity as measured by the Hurst exponent (*H*) of electrophysiological signals and fMRI BOLD signals has been a hallmark of queries related to the 'criticality hypothesis' within the field of cognitive neuroscience, which models brain at rest as a network configured to operate near a critical state. In this dissertation I investigated the significance of *H* in EEG and fMRI data with regards to cognitive processes involved in working memory and learning. In chapter 1, I utilized global *H* suppression in EEG to distinguish working memory load from cognitive effort. Results from two visual working memory experiments with varying memory set size provided evidence for the suppression of scale-invariance in EEG due to task difficulty that continues even after working memory capacity has been reached. In contrast, task performance and oscillatory signals of working memory load both plateau beyond working memory capacity. This suggests that *H* suppression may be used to reliably indicate an effortful state. In chapter 2, I used *H* measured with fMRI data to predict learning in a dual n-back (DNB) working memory task. I hypothesized that learning potential is higher when brain networks are poised closer to a critical state, and thus higher *H* can be used to predict more learning and improvement on cognitive tasks. The results show that higher *H* during learning distinguished task improvers from non-improvers. As a comparison, neither baseline task performance nor fMRI functional connectivity strength reliably classified improvers vs. non-improvers. I then successfully cross-validated the H-based model from the DNB dataset on an independent fMRI dataset of participants performing a completely different working memory task (word completion). Taken together, these results suggest that scale-free brain activity can be used as an objective measure of an individual's cognitive state and provide support for the utility of the criticality hypothesis.

Chapter 1:

# Distinguishing cognitive effort and working memory load


## Abstract

Despite being intuitive, cognitive effort has proven difficult to quantify. In the current study we validated the correspondence between scale-invariance (*H*) of cortical activity recorded by EEG and task load during two working memory (WM) experiments with varying set sizes. We used this neural signature to disentangle cognitive effort from the number of items in WM. Our results showed monotonic decreases in *H* with increased set size, even after set size exceeded WM capacity. This behavior of *H* contrasted with behavioral performance and an oscillatory indicator of WM load (i.e., alpha-band desynchronization), both of which showed a plateau at difficulty levels surpassing WM capacity. This is the first reported evidence for the suppression of scale-invariance in EEG due to task difficulty, and our work suggest that *H* suppression may be used to quantify changes in effort even when working memory load is constant and at maximum capacity.

## Introduction

Cognitive effort is a seemingly intuitive aspect of cognition, yet has proven difficult to quantify because of gaps in both theory and practice. Some researchers, at least implicitly, equate mental effort with working memory (WM) load (Garbarino & Edell, 1997; Kitzbichler, Henson, Smith, Nathan, & Bullmore, 2011), whereas others see WM load and effort as confounded measures that could, in theory, be separated (Vogel & Machizawa, 2004). Practically, the literature lacks a sensitive and specific neural signature that can be used as a marker of mental effort. As a result of these gaps, the literature has produced many competing operational definitions of effort (Otto & Daw, 2018; Paas, Tuovinen, Tabbers, & Gerven, 2003; Westbrook & Braver, 2015). Therefore, the identification of a reliable neurobiological marker specific to cognitive effort would facilitate the operationalization of cognitive effort for both theoretical and applied research. Within the context of neuroimaging of WM tasks, a core challenge for identifying a neural signal of effort involves disentangling effort signals from WM storage signals. This is because, until maximum WM capacity is reached, exerting more effort often enables meeting larger WM demands. To address this challenge, we took advantage of results from two well-characterized research domains. By combining what is known from fMRI studies of effort signals with what is known from EEG studies of working memory storage signals, we were able to identify a specific neural marker of effort in EEG, distinct from working-memory storage signals.

fMRI research has revealed a potential neural signature for quantifying effort: scale-invariance of the broadband signal. Scale-invariance in biological signals (sometimes also called scale-free or fractal scaling) refers to a property of signals where all measured time

scales contribute to a signal of interest, with no particular timescale having a dominant contribution. It is a property of "long-memory" systems with persistent autocorrelations and is typically modeled as a power-law relationship between frequency *f* and power spectral density PSD(*f*) of the signal, $PSD(f) \sim |f|^{-\beta}$ , for scaling parameter $\beta \geq 0$. This is often expressed in terms of the Hurst exponent (*H*), which quantifies temporal dependence of signals, with higher values denoting a more scale-free signal. Scale-free dynamics are a feature of many biological systems under complex control including the human nervous system (Werner, 2010) and a breakdown of fractal scaling often signifies increased physiological stress (Goldberger et al., 2002); for other interpretations of *H* in neural signals see (von Wegner, Laufs, & Tagliazucchi, 2018). Research on scale-free dynamics of fMRI timeseries demonstrates that global Blood Oxygenation Level Dependent (BOLD) activity of the brain becomes less scale-free (lower *H*) in the presence of cognitive tasks and other modulators of cognitive effort (Barnes, Bullmore, & Suckling, 2009; Churchill et al., 2016; He, 2011). Specifically, fMRI timeseries have lower *H* when: 1) performing hard vs. easy perceptual decision tasks, (Churchill et al., 2016), 2) performing a visual detection task vs. open-eyes rest (He, 2011), 3) performing n-back task versus rest (Barnes et al., 2009), 4) performing novel tasks vs. more familiar tasks (Churchill et al., 2016), and 5) when participants were under physical and mental burden (Churchill et al., 2015). These findings suggest that suppression of *H* may be a generalizable neuroimaging marker of increased cognitive effort.

EEG research on visual working memory (VWM) points to a capacity limit (referred to as *K*) beyond which the individual cannot maintain any more mental representations of the presented items. Specifically, recent research in VWM suggests a limit of 3-4 items for *K*

(Adam, Vogel, & Awh, 2017; Fukuda, Awh, & Vogel, 2010; Luck & Vogel, 2013; Rouder et al., 2008), but see (Alvarez & Cavanagh, 2004)). Additionally, this research has suggested that the primary role of alpha band (8-12 Hz) oscillations (α) in the context of VWM is to maintain distinct working memory representations rather than to suppress irrelevant information (Foster & Awh, 2019). This indicates that as the number of relevant items in VWM increases, α will systematically decrease until WM capacity (*K*) is reached (Adam, Robison, & Vogel, 2018; Fukuda, Kang, & Woodman, 2016; Fukuda, Mance, & Vogel, 2015). Therefore, translating the fMRI work examining *H* and cognitive effort to EEG experiments on oscillatory activity and *K* can provide us with the framework needed to investigate the distinction between cognitive effort and WM load. Pertinently, previous literature has shown that BOLD fMRI signal fluctuations are linked to scale-free fluctuations in EEG measurements of neural activity (Van de Ville, Britz, & Michel, 2010). As such, an effort-related suppression in scale-invariance would also be expected at the electrophysiological timescale. Additionally, studying these broadband effects with EEG will potentially be more fruitful than with fMRI since this method overcomes the limited range of timescales that can be examined for *H* in fMRI due to its slow sampling rate. To our knowledge, this relationship between suppression of *H* and cognitive effort beyond *K* has not yet been investigated using EEG, where it would provide a critical validation of the fMRI findings using a more direct measure of neural activity and a wider range of accessible timescales.

In the current study, we analyzed two VWM EEG experiments including a 'Remember N' task (Experiment 1) and a Discrete Whole-Report task (Experiment 2)[1]. In both experiments, a memory array was presented to participants while they maintained

[1] Aspects of experiment 1 and 2 were previously published in (Mance, 2015) and (Adam, Robison, & Vogel, 2018), respectively.

fixation on the center of the screen. Memory load was parametrically varied (N = 1, 2, 3, or 6 items)[2]. We hypothesized that scale-invariance (*H*) of the EEG signal during the retention interval would decline parametrically with increasing task load, even beyond *K* (i.e., beyond 3-4 items). In contrast, α suppression has been shown to plateau for set sizes beyond *K*. As such, we further predicted that the pattern of *H* across set sizes would significantly diverge from the pattern of α across set sizes as α suppression would *not* continue to decrease beyond *K*. The above predictions assume cognitive effort to be distinguishable from the amount of information in WM. In summary, we propose that (1) global scale-invariance of cortical brain activity as recorded by EEG can be used as a metric of cognitive effort, and (2) this broad-band signal characteristic can dissociate VWM load from the effort exerted for the task at hand, thus providing a neurobiological dissociation between effort and information in WM.

## Experiment 1 Methods

### Participants

Experiment 1 included 31 participants (18-35 years old; 17 female) from the University of Oregon and surrounding community (Mance, 2015). A total of 6 were excluded from analyses because of excessive EEG artifacts (see *Artifact Rejection*), leaving a final sample of 25 participants. Participants gave written informed consent, and experimental procedures were approved by the University of Oregon's Committee for the Protection of Human Subjects (CPHS) and Institutional Review Board (IRB). All participants

[2] For experiment 2, N = 1, 3, and 6.

had normal or corrected-to-normal visual acuity and reported no history of neurological disorders.

**Stimuli**

Participants were seated ~100 cm from a 17-in. cathode ray tube monitor. Stimuli were rendered using the Psychophysics toolbox (Brainard, 1997; Pelli, 1997). Participants remembered colored squares presented on a medium gray background (RGB = 120 120 120) while maintaining fixation on a small white dot (0.2°). A pool of eight distinct colors: red (RGB = 255 0 0), green (0 255 0), blue (0 0 255), yellow (255 255 0), magenta (255 0 255), cyan (0 255 255), white (255 255 255), and black (1 1 1) were used to choose the colors from in each trial. Each square subtended 1°, and each square was placed at one of 32 locations on the screen (equally spaced grid of 4 x 8 locations, placed within a portion of the display subtending 8.1° to the left or right of fixation and 4.7° above or below fixation.

**The Remember N Task**

On each trial, participants were first given a cue which indicated how many items they should encode from the upcoming display (e.g., "Remember 3") and pressed the spacebar to initiate the trial. The cue presentation was un-speeded but had a minimum duration of 600 ms. After a blank baseline (1,200 ms), participants briefly viewed six colored squares (150 ms) and remembered all or some of these squares across a delay (1,150 ms). Participants were instructed to try their best to only remember the cued number of items and to ignore the rest (Figure 1.1), but they were not instructed about which particular items to remember (they could freely choose). To respond, participants clicked the color in the response grid corresponding to the color remembered at that

location. During the response, participants only had the option to respond to as many items as they were cued to remember (for example, if the cue was "Remember 1", they could only make one response during the recall phase). After the participant had made all responses the cue for the next trial appeared after 500 ms. There were a total of 150 trials per set-size (30 blocks of 20 trials, ~2.5 hours).

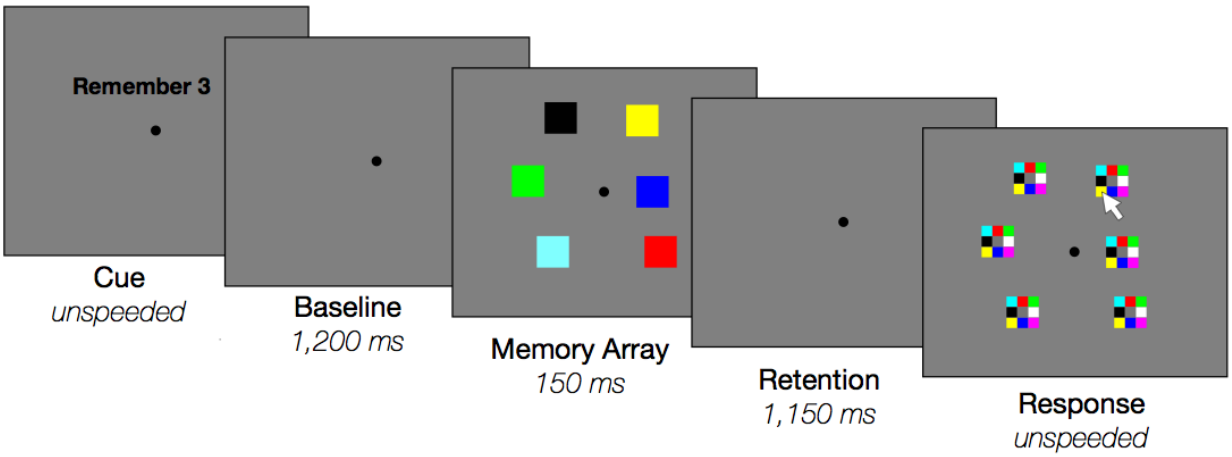


**Figure1.1.** Experiment 1: "Remember N" task procedures. At the beginning of every trial, participants were cued about how many items to remember from the upcoming memory array. Memory arrays always contained six items shown in random locations. At response, participants only recalled as many items as they were asked to remember.

**Data Acquisition and Analysis**

Data were acquired with an SA Instrumentation amplifier with a band-pass of .01-80 Hz and digitized at 250 Hz in LabView 6.1. We measured EEG from 20 tin electrodes mounted in an elastic cap (Electrocap International, Eaton, OH) at International 10/20 sites F3, Fz, F4, T3, C3, Cz, C4, T4, P3, Pz, P4, T5, O1, and O2 and five nonstandard sites: OL midway between T5 and O1, OR midway between T6 and O2, PO3 midway between P3 and OL, PO4 midway between P4 and OR, and POz midway between PO3 and PO4 (Figure S1.1). All sites were recorded using a left-mastoid reference and re-referenced offline to the

algebraic average of the left and right mastoids. The vertical electrooculogram (EOG) was recorded from an electrode placed ~1 cm below the right eye. The horizontal EOG was recorded from electrodes placed ~1 cm lateral to the external canthus of each eye. Electrode impedances were kept below 3 kΩ. Participants were instructed not to move their eyes or blink during the trial until the test array appeared on the screen. Trials including horizontal eye movements, blinks, blocking (amplifier saturation after drift), or excessive noise were excluded from analysis (mean = 16.8% of trials).

**Artifact Rejection**

For horizontal eye movement rejection, we used a split-half sliding window approach (window size = 150 ms, step size = 10 ms, threshold = 20 μV) on the HEOG signal, where a 150 ms time window was slid in steps of 10 ms from the beginning to the end of the trial. If the change in voltage from the first half to the second half of the window was greater than 20 μV, it was marked as an eye movement and rejected. We also used a sliding window step function to check for blinks in the VEOG (window size = 100 ms, step size = 10 ms, threshold = 40 μV). For blocking rejection, we slid a 200 ms time window in steps of 50 ms and excluded trials for blocking if any EEG electrode had at least 20 consecutive time-points (i.e. 80 ms) that were within 1 μV of each other. We excluded trials for excessive noise if any electrode had peak-to-peak amplitude greater than 200μV within a 15 ms time window. Data were visually inspected to confirm that rejection criteria were working as expected; some additional trials were manually rejected. Six participants were excluded for excessive artifacts (fewer than 70 good trials per condition on average, remaining n = 25). After rejection, included participants had an average of 110 trials per condition (SD = 22.5).

**Estimation of α Power**

To estimate alpha power (8-12 Hz), we first band-pass filtered the raw EEG signal for each trial and electrode using a two-way least-squares FIR filter , 'eegfilt.m', (Delorme & Makeig, 2004). We calculated instantaneous power with the MATLAB Hilbert transform ('hilbert.m'). Because we were interested in event-related changes to alpha power as a function of memory load, we analyzed percent change in alpha power relative to the memory array onset. For each participant and electrode, we first averaged single-trial power across each load condition, then calculated the percent change in alpha power for each condition relative to a baseline period (500 ms to 100 ms before the memory array).

**Estimation of Scale-Invariance (*H*)**

Scaling analyses of temporal signals seek to determine whether all measured frequencies (or timescales) contribute to the signal of interest. Scale-invariance occurs when no particular frequency (or timescale) has a dominant contribution to the signal, implying that the signals have long-range temporal dependency. This dependency is indexed via the Hurst exponent *H*, where $H \leq 0.5$ indicates short-range dependency, $H=0.5$ denotes an uncorrelated process, and $H \geq 0.5$ indicates long-range dependency, with $H=1$ indicating complete scale-invariance.

While there exist many different methods to estimate *H*, the wavelet leader multifractal (WLMF) formalism has emerged as a powerful technique that is highly efficient and robust to signal non-stationarity (Jaffard, Lashermes, & Abry, 2007). We applied the WLMF method on the EEG signal during retention interval (after memory array and before response) to quantify the scale-invariance of the EEG signal during maintenance. The

wavelet transform uses translated and dilated versions of a basis function $\Psi([t-k]/a)$ to analyze the signal of interest at different delays and time scales. The wavelet coefficient $d_x(a,k)$ measures signal energy present at delay $k$ and time scale $a$ by calculating the integral:

$$d_x(a,k) = \frac{1}{a}\int x(t)\Psi\left(\frac{t-k}{a}\right)dt$$

At a range of dyadic scales, i.e., $a = 2^j$ for integer $j$. Wavelet leaders $L_x(a,k)$ are subsequently calculated as the largest coefficient value $|d_x(a',k')|$ within a narrow temporal neighbourhood of $k$, for any scale $a' \leq a$. Multifractal scaling is then defined by the function:

$$\frac{1}{K}\sum_k \left|L_x(2^j,k)\right|^q = C_q 2^{j\varsigma(q)}$$

Which describes wavelet power as a function of time scale, for a range of different scaling exponents $q$, in terms of a characteristic function $\varsigma(q)$. Typically parameterized as a polynomial expansion $\varsigma(q) = \sum_p c_p(q^p/p!)$, the log-cumulants $c_\mathrm{p}$ define the scaling behavior of the signal $x(t)$. In this study, we focused on first-order cumulant $c_1$, which is closely linked to the monofractal scaling parameter $H$ (Wendt, Abry, & Jaffard, 2007). An exploratory analysis of the higher-order cumulants ($c_2$ and $c_3$) did not show a relationship between them and the memory load in our two experiments.

**Canonical Correlation Analysis**

In a canonical correlation analysis (CCA), two sets of variables are related together (as opposed to many variables to a single dependent variable) and the degree of relationship between the two sets of variables is assessed (Hotelling, 1936). An

advantage of multivariate methods such as CCA to univariate methods is that they reveal the linear relationship between all spatial (every electrode) and task-related (every task load level) contrasts simultaneously without the multiple comparison problem or the need for coming up with a-priori contrasts.

For two datasets X and Y, CCA identifies pairs of canonical weighting vectors $w_x$ and $w_y$ which produce corresponding linear latent variables $l_x = Xw_x$ and $l_y = Yw_y$, such that correlation $\rho_{XY} = corr(l_x, l_y)$ is maximized and orthogonal to any other latent variable pairs. We used CCA to find latent variables that relate either scale-invariance (*H*) of the 20 electrodes (bottom set of variables in Figure 1.2A) to the task loads (top set of variables in Figure 1.2A) or the alpha desynchronization of the 20 EEG electrodes (bottom set of variables in Figure 1.2B) to the task loads (top set of variables in Figure 1.2B). Each task load (i.e., set size) was dummy coded as a binary variable, so the number of total latent variables possible was N-1 (i.e., the rank of the smaller set of variables), where N is the number of levels of load in each experiment (N = 4 in experiment 1; N = 3 in experiment 2). Only the primary latent variables in the experiments are shown in the results because no secondary (or tertiary for Exp. 1) latent variables were large enough ($\rho_{XY} > 0.25$) in either experiment to be considered meaningful. Small effects, conventionally in the range of r = [0.15 0.25] (Kirk, 2012), are not of interest here because a biomarker with smaller than medium effect size (i. e., r = 0.25) (Kirk, 2012) will likely not have practical utility due to lack of sufficient sensitivity. Each electrode's or task load's contribution to the latent variable is represented by the canonical weight of the observed variable which is the Pearson correlation coefficient of that variable with the latent variable. The stability of the latent variables is evaluated by the error bars of the canonical weights on both left

and right sets, which are the 95% confidence intervals calculated by bootstrapping the data (3000 samples with replacement) to create distributions for the canonical weights similar to (Kardan et al., 2017). The strength of the association between the two sets in a latent variable is represented by the correlation between the two sides (double sided arrows in Figure 1.2). As such, the relationship represented in a latent variable is considered strong and stable if the correlation is large ($\rho_{XY} > 0.4$) *and* there is at least one variable in each side (i.e., at least one electrode and one task load) whose weight reliably differs from zero across the bootstrapped samples (i. e., omnibus non-parametric $p<0.05$).

**Statistical Power**

Following our hypothesis regarding relationships between electrode data and set sizes, we simulated the CCA analysis to estimate statistical power for detecting a true correlation between electrodes' data and a contrast delineating a set size from the other set sizes (e.g., contrast C = [-1 -1 +1 -1] delineates set size 3 in Experiment 1). This was done in 5 steps. First, we generated a random Gaussian variable Norm(0,1) for *N* levels of set size and 20 electrodes for *n* participants. Second, to create a true correlation between the generated electrodes data and a set size contrast, we introduced a bias (i. e., a uniformly distributed random variable with an expected value above zero) in the generated electrode data for one set size (chosen randomly). We did this by adding a $\beta_{bias}$ * Unif(0,1) to the generated data for that set size and subtracting $\beta_{bias}$ * Unif(0,1) from the other set sizes. This produces a difference of $\beta_{bias}$ in the expected values of the electrode data for the biased set size compared to electrode data of other set sizes. Third, through trial and error iterations, we found that $\beta_{bias} = 0.62$ induced correlations that closely resembled the minimum effect size of interest (r = 0.25, see CCA analysis). This value of $\beta_{bias}$ resulted in

true correlations in the range of r = [0.24  0.26] between the set size contrast (i. e., dummy variables coding 1 for the biased set size and -1 for the other set sizes) and the generated electrodes data for Experiment 1. Fourth, we then applied the CCA procedure explained in the previous section[3] to the generated data to determine whether the CCA weight for the biased set size in the primary latent variable was found to be significant at $\alpha = 0.05$. Finally, we repeated step (4) 500 times, with $N = 4$ and $n = 25$ to simulate the final sample size for Experiment 1. Statistical power was estimated to be 0.78 by calculating the proportion of times in the 500 runs where the induced correlation was found to be significant in the simulated CCAs.

## Experiment 1 Results

The average number of correctly reported items was 0.96 (SD = 0.03) items, 1.84 (SD = 0.13) items, 2.35 (SD = 0.35) items, and 2.29 (SD = 0.44) items for set sizes 1, 2, 3, and 6, respectively. This pattern of performance is consistent with our assumption that working memory capacity in this task would be limited to around 3 items; when the set size increased from 3 to 6 items, the number of correctly reported items did not increase (decrease of 0.06 items, p = 0.771).

### CCA Results for Scale-Invariance

In the Remember N task, the primary latent variable from the CCA showed a strong ($R^2 = 0.254$, $p < 0.001$) and stable relationship (see Figure 1.2A bottom panel) between the number of to-be-remembered items and the scale-invariance of the EEG signal during retention, where a global decrease in *H* (especially in occipital and parietal regions, see

[3] The only difference being that instead of 3000 resamples for each CCA, we did 300 resamples to cut down processing time in each loop of the simulation.

Figure 1.2B) tracked increases in task load. Importantly, the decrease in scale-invariance corresponded monotonically to task load, where each load level had a significantly larger canonical weight than the previous one (except for when going from load 1 to 2, perhaps due to both loads being relatively easy). The canonical weights were $r_1 = -0.63$, $r_2 = -0.39$, $r_3 = 0.24$, and $r_6 = 0.78$ for each set size, respectively. The significant increment from load 3 to 6 (one-sided arrow in Figure 1.2A top) follows our hypothesis that *H* is sensitive to the exerted cognitive effort rather than the capacity limits of visual working memory.

**CCA Results for α Desynchronization**

As shown in Figure 1.2C, the primary CCA latent variable relating change in α power during the retention period and task load showed a strong and stable relationship ($R^2 = 0.239$, $p < 0.001$) between the two sets of variables. As expected, lower α power in the posterior electrodes (occipital and parietal, see Figure 1.2D) corresponded to higher task load. The canonical weights were $r_1 = -0.83$, $r_2 = -0.09$, $r_3 = 0.66$, and $r_6 = 0.25$ for each set size, respectively. Importantly, the correspondence was not monotonic as indicated by the canonical weight for load 6 not being larger than canonical weight for load 3 (in fact it was marginally smaller; non-parametric $p = 0.057$). Thus, the relationship between alpha power and task load diverged from the monotonic correspondence between *H* and task load that we reported above. This bifurcation (see one-sided arrows in Figure 1.2A and C top panels) in the relationship between task load and *H* versus alpha was statistically significant (Fischer's $Z = 2.66$, $p = 0.008$), supporting our hypothesis that posterior α desynchronization is sensitive to working memory load rather than cognitive effort. Together, the results from the first experiment suggest that working memory load and

cognitive effort are distinguishable and can be tracked by alpha band desynchronization versus broad-band characteristics of the EEG signal (*H*).

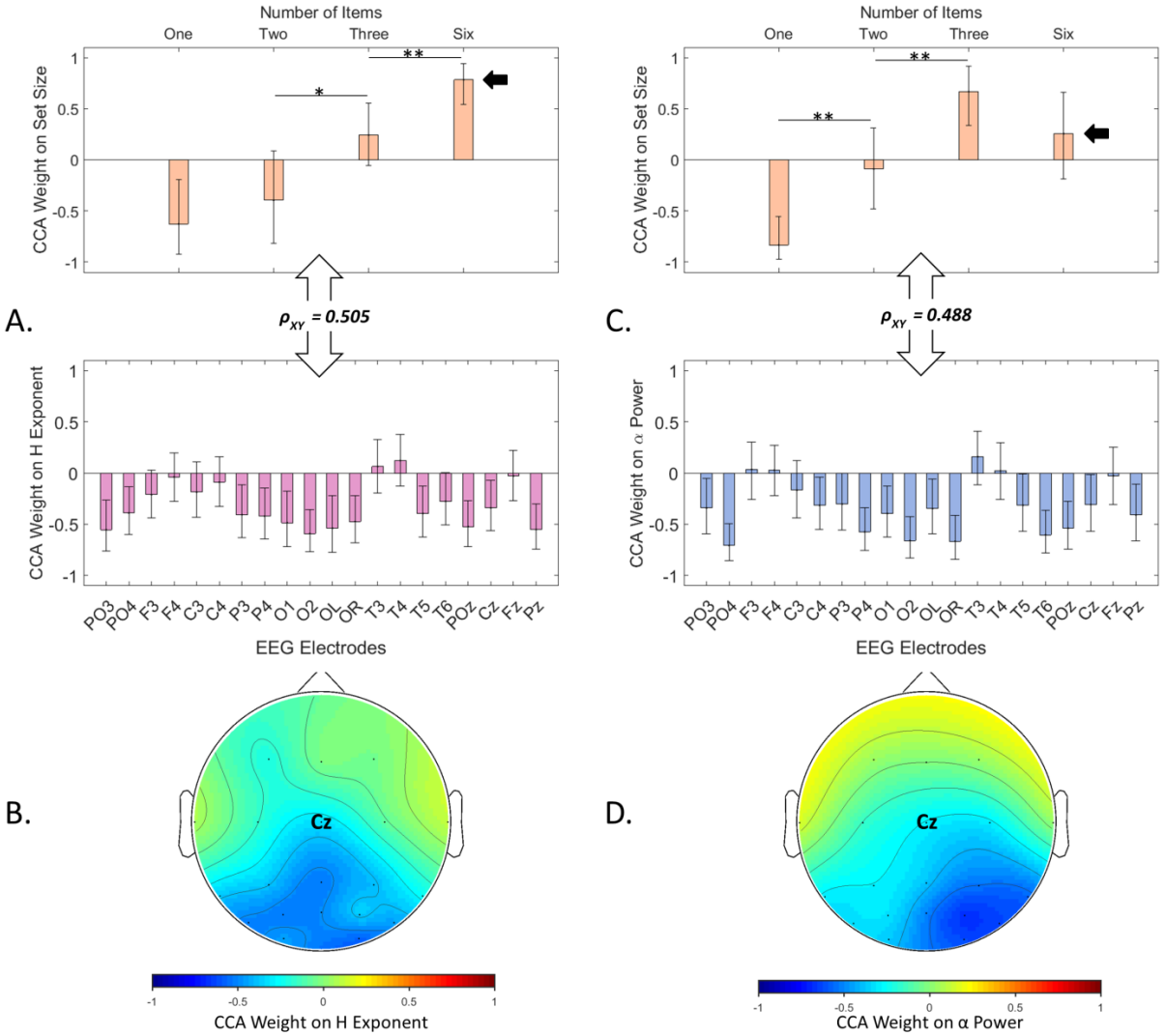


**Figure 1.2.** The primary latent variables of the CCA analysis for the Remember N task in Experiment 1. (A) The primary relationship between scale-invariance (*H*) of the EEG electrodes during the retention period (pink) with the number of items to remember (orange). The double-headed arrows show the strength of the correlation between the bottom set (electrodes) and the top set (task loads). The vertical axis in each panel shows the contribution of an electrode (bottom) or a specific task load (top) to the latent variable as indicated by the size of its normalized CCA weight. The error bars show bootstrapped 95% confidence intervals around the means for the weights. The asterisks show statistical significance in the difference between weights of adjacent levels of task load (i.e., 1 item to

**[Figure 1.2. continued]** 2 items, 2 items to 3 items, and 3 items to 6 items), *p < 0.05 and **p <0.01. (B) Topographic demonstration of the CCA weights on the *H* exponent. (C) The primary relationship between the desynchronization of α band power from baseline during the retention period (blue) with the number of items to remember (orange). One-sided arrows demonstrate difference in CCA weight for set size 6 in the relationship between task load and *H* versus task load and alpha power. (D) Topographic demonstration of the CCA weights on alpha power.

## Experiment 2 Methods

### Participants

A group of 31 participants (ages between 18 to 35, 12 women) were recruited from the University of Oregon and surrounding community (Adam et al., 2018). All participants had self-reported normal or corrected-to-normal visual acuity and normal color vision. All participants gave informed consent and completed the 3-hr session for $30 in compensation. Four participants were excluded from analyses for having fewer than 70 trials per condition on average after artifact rejection (remaining n = 27). After rejection, included participants had an average of 148 trials per condition (SD = 39.5).

### Stimuli

Stimuli and procedures were similar to Experiment 1. The key difference was that that for this lateralized whole-report task, participants were cued to attend either the left- or right-half of the display before the onset of the memory array. They were asked to remember all items presented in the cued hemifield. The cue was a small pink and green diamond, approximately 0.2° tall by 0.4° wide and was presented 0.4° above the fixation cross. Participants remembered colored squares presented on a medium gray background (RGB = 127.5 127.5 127.5) while maintaining fixation on a small black dot (0.12°). A pool of nine distinct colors: red (RGB = 255 0 0), green (0 255 0), blue (0 0 255), yellow (255 255

0), magenta (255 0 255), cyan (0 255 255), orange (255 128 0), white (255 255 255), and black (1 1 1) were used to choose the colors from in each trial. Each square subtended 1.2° and they could appear anywhere within a portion of the display subtending 7.0° to the left or right of fixation and 5.2° above or below fixation as long as there was a minimum distance of at least 1.5 squares between the centroids of any two squares.

**Discrete Whole-Report Task**

Each trial began with a blank inter-trial interview (500 ms) followed by the spatial cue (1100 ms) which indicated which side of the screen to attend. After the cue period ended, a memory array containing an equal number of items on both sides of the screen (cued and uncued) was presented for 250 ms. The colors of squares in the memory array were chosen without replacement within each side (i.e., all cued colors were unique but might be repeated on the uncued side of the display). After encoding, participants remembered the items across a blank delay of 1300 ms. At test, a 3×3 matrix of the nine possible colors was presented at the location of each item on both the attended and unattended side. Similar to the Remember N task in Experiment 1, participants were instructed to click the color in each matrix corresponding to the color presented at the location (see Figure 1.3). The response period ended after participants made a response for all items on the attended side. Participants clicked the mouse to initiate the beginning of the next trial.

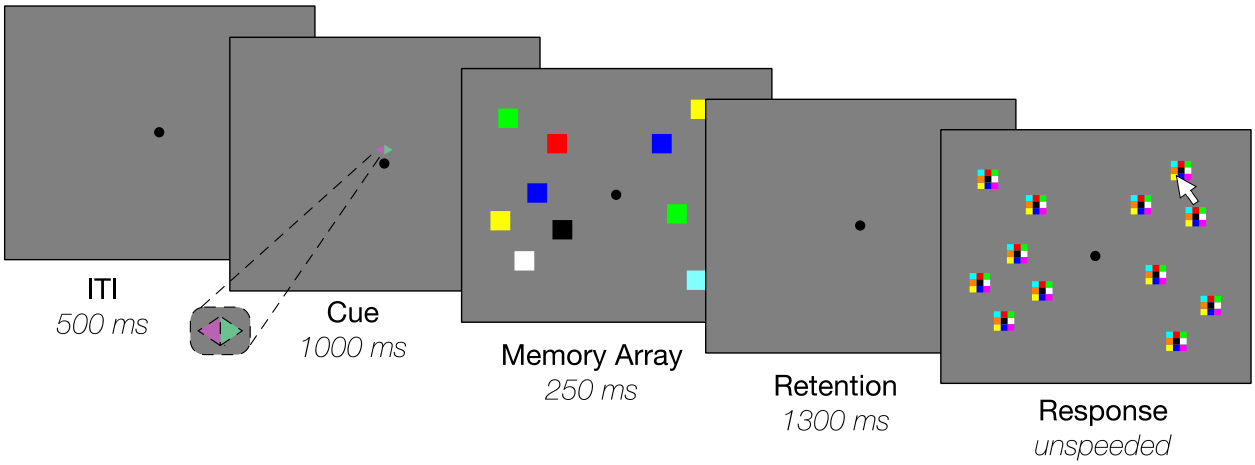


**Figure 1.3.** Experiment 2 "Whole-Report" task procedures. At the beginning of every trial participants were given a cue indicating which side of the screen to remember from the upcoming memory array. Memory arrays could contain 1, 3, or 6 items shown in random locations on each side; at response participants only recalled items from the cued side.

### Data Analysis and Statistical Methods

Artifact rejection, alpha power analysis, wavelet analysis for *H,* and the CCA analysis were the same as described in Experiment 1[4]. For statistical power, the parameters of the simulation were set at N = 3, n = 27, and $\beta_{bias}$ = 0.60 for Experiment 2, which determined a statistical power of 0.72 for the analysis. The simulation showed that Experiment 2 would have sufficient power (conventionally 0.8) to detect effects only if they are equal to or larger than r = 0.29.

## Experiment 2 Results

The average number of correctly reported items was 0.95 (SD = 0.04) for set size 1, 2.41 (SD = 0.33) for set size 3, and 2.53 (SD = 0.53) for set size 6. This, again, indicates that

[4] Analysis where we only calculated alpha desynchronization for trials ipsilateral to lateralized electrodes yielded very similar results.

average *K* was still less than 3 even for 6 items, although performance was slightly better for 6 items (0.12 items increase, $p = 0.085$).

**CCA Results for Scale-invariance**

Replicating the Remember N task, the primary latent variable from the CCA in the lateralized Whole-Report task showed a very strong ($R^2 = 0.416$, $p < 0.001$) and stable relationship between the number of presented items to be remembered in the task and the scale-invariance of the EEG signal during retention (Figure 1.4A). Again, a global decrease in *H* tracked increases in the task load. The canonical weights for each set size in this latent variable were $r_1 = -0.78$, $r_3 = -0.13$, and $r_6 = 0.91$, respectively. Importantly, the decrease in scale-invariance changed monotonically with task load, where the canonical weight for each load level was significantly larger than the previous one including from load 3 to 6. This follows our hypothesis that *H* is sensitive to the exerted cognitive effort in visual working memory tasks.

**CCA Results for α Desynchronization**

The primary CCA latent variable relating change in α power and task load was not stable, as the 95% confidence intervals for all of the electrodes contained zero (Figure 1.4C bottom). The task load levels were not significantly different from one another (Figure 1.4C top), although there was a numerical trend of suppression of α power for 6 items compared to 1 item. Thus, the relationship between task load and alpha power did not follow the pattern we observed in Experiment 1. However, since the latent variable was not stable, the canonical correspondence for α suppression in this experiment was not conclusive with regards to our hypothesis about distinguishing working memory load from cognitive effort.

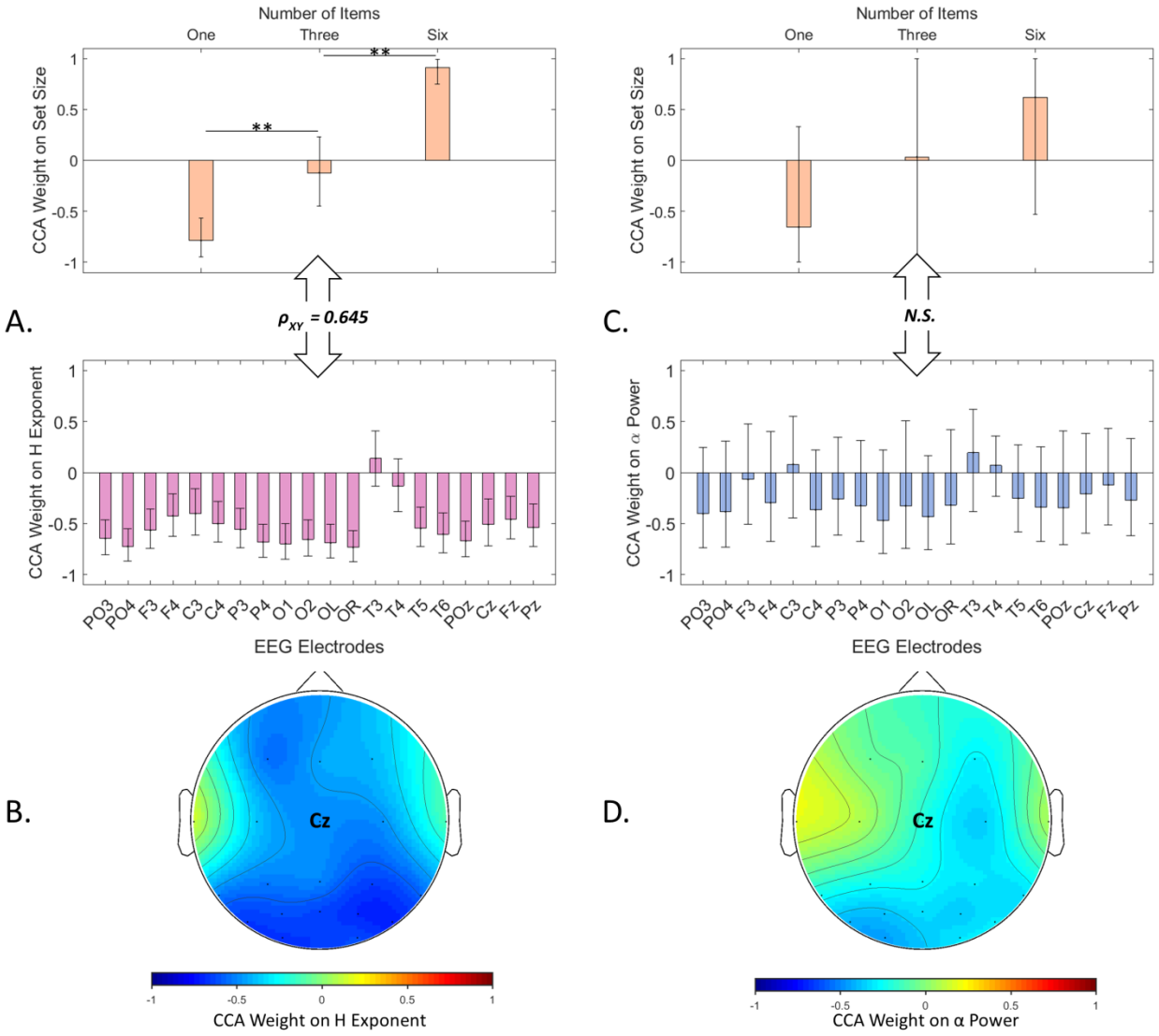


**Figure 1.4.** The primary latent variables of the CCA analysis for the Whole-Report task in Experiment 2. (A) The primary relationship between the scale-invariance (*H*) of the EEG electrodes during retention period (pink) with the number of items to remember (orange). The double-headed arrows show the strength of the correlation between the bottom set (electrodes) and the top set (task loads). The vertical axis in each panel shows the contribution of an electrode (bottom) or a specific task load (top) to the latent variable as indicated by the size of its normalized CCA weight. The error bars show bootstrapped 95% confidence intervals around the means for the weights. The asterisks indicate statistical significance in the difference between weights of adjacent levels of task load (i.e., 1 item to 2 items, 2 items to 3 items, and 3 items to 6 items), where *p < 0.05 and **p <0.01. (B) Topographic demonstration of the CCA weights on the *H* exponent. (C) The primary relationship between the desynchronization of α band power from baseline during

**[Figure 1.4. continued]** retention period (blue) with the number of items to remember (orange). (D) Topographic demonstration of the CCA weights on alpha power.

## Discussion

In this study, we found a monotonic correspondence between scale-invariance of cortical activity recorded by EEG and task load across two experiments. This is the first reported evidence for the suppression of scale-invariance due to task difficulty as measured with EEG (a relatively high frequency signal), lending support to the previous literature relating fractalness of BOLD activity (a very low frequency signal) to task difficulty. Importantly, we used this signal characteristic in an attempt to address an elusive question of what distinguishes an effortful task from an easy one, and whether, in the context of doing a visual working memory task, there is more to cognitive effort than working memory load (Heitz, Schrock, Payne, & Engle, 2008). Our results suggest that increases in *H* with task load may be contrasted with behavioral performance, where the number of recalled items hardly increased after intermediate difficulty levels, if not completely plateaued. This suggests that *H* is more sensitive to neural processes associated with task difficulty than with overt performance. Consequently, by showing a neurobiological dissociation between cognitive effort and the amount of information available for manipulation in working memory, our results support the theoretical account of cognitive effort that distinguishes it from information in working memory. One potential explanation for why an effortful state would be reflected in *H* suppression of brain signals is the loss of self-organized criticality exhibited by a healthy brain in neutral state (Kitzbichler, Smith, Christensen, & Bullmore, 2009), due to disproportionate allocation of

resources to a specific cognitive demand. When *H* is not suppressed, small perturbations can lead to large changes in brain state (Chialvo, 2004), thereby enabling rapid adaptability to heterogeneous external demands (Gisiger, 2001). Locking into an effortful state sacrifices the ability of the brain to adapt to other demands represented by a loss of criticality in brain networks, which exhibits itself in *H* suppression.

Unlike α suppression, the differences in the design of the two experiments did not change the behavior of *H* with regards to task load. Specifically, the differences in the experimental designs could test if certain aspects of the tasks such as the perception of items, the number of internal representations, or the inhibition of the distracting information is responsible for the suppression of scale-invariance. For example, in the Remember N experiment when participants were cued to only remember one item, the other five items on the screen were essentially distractors. If scale-invariance was primarily driven by inhibition of irrelevant information, the relationship between set size and *H* should have been in the opposite direction between the two experiments, since the greatest amount of suppression is required in set-size 1 trials in Experiment 1 (five distractors) and set-size 6 in Experiment 2 (six distractors). If *H* was modulated by the visual display imbalance between the different set sizes, then we should have only seen a correspondence between scale-invariance and set size in the whole-report task (Experiment 2) and not in Experiment 1 since the number of items on the screen was constant (6 items).

We found *H* suppression to be more related to task difficulty than to task performance. Intuitively, factors such as motivation, fatigue, and anxiety can play roles in increased cognitive exertion in the absence of any specific improvements in behavior. The

logic here is that higher levels of motivation, and/or lower levels of fatigue or anxiety, can increase the maximum capacity for expending effort differentially from their effect on working memory capacity (if any, see (Bonner & Sprinkle, 2002; Botvinick & Braver, 2015)). Previous fMRI studies have shown that fatigue due to physical burdens such as chemotherapy could disrupt brain function in a manner that is unrelated to working memory performance (Kardan, Adam, et al., 2019). Moreover, such physical burdens in this cohort have been shown to alter the scaling properties of fMRI timeseries (Churchill et al., 2015).

Importantly, the scale-invariance of EEG signals in our experiments is a broad-band characteristic of the signal and even though it is (anti)correlated with narrow-band oscillations such as theta, alpha, and beta band power of the EEG signal (see supplementary Figure S1.2), its relationship with task difficulty was not driven by any of these specific narrow-band oscillation correlates (regarding cognitive tasks modulating beta and theta oscillations see (Engel & Fries, 2010; Sederberg, Kahana, Howard, Donner, & Madsen, 2003). We demonstrated this by applying CCA to investigate the correspondence between theta (4-7 Hz) as well as beta (13-30 Hz) band powers of the electrodes with the set sizes in both experiments similar to the analyses done for α and *H*. Neither theta nor beta band powers mimicked *H* suppression's relationship with set size (see supplementary results: *CCA for theta and beta bands*).

In conclusion, in this study we used the time scale-invariance characteristic of the EEG signal (*H*) to dissociate visual working memory load from the cognitive effort exerted for the task at hand. Our work further demonstrated the utility of *H* as a neuromarker of cognitive effort. These results have theoretical implications for research on motivation and

cognitive fatigue, as well as practical implications for education. Regarding theory, we ruled out interpretations of cognitive effort that equate it with working memory load. Regarding application, the relatively accessible *H* of EEG signal can serve as robust neuro-feedback in educational interventions by indicating individual differences in effort towards solving specific problems, as well as tracking cognitive fatigue over time and thus signaling changes in motivation within an individual.

Chapter 2:

## No Hurst for the weary: Lower fMRI scale-invariance predicts lack of improvement in working memory performance

**Abstract:**

Suppression of scale-invariance (H) in both EEG and fMRI brain signals have been linked to exertion of higher cognitive effort while performing working memory (WM) tasks. Thus, we interpret an effortful state as a sub-critical 'cognitive state' in brain networks indicated by lowered H. Consequently, we hypothesized that it is possible to predict an individual's level of learning and improvement in performance of a WM task by assessing their 'cognitive state' during learning as indexed by the scale-invariance of their brain activity during the learning period and consolidation interval preceding the final task performance. In this study, participants (n = 56) preformed an audio-visual Dual N-Back (DNB) task, followed by passive viewing of videos (as rest break) and then a final DNB again, all while in an MRI scanner. We then categorized the participants into two groups of improvers and non-improvers based on their change in DNB performance, and measured both whole-brain and ROI-specific H of fMRI timeseries in each run. We found that higher H during learning and subsequent resting period distinguishes improvers from non-improvers despite similar baseline DNB performances. As a comparison, neither baseline DNB performance nor fMRI functional connectivity strength was enough to reliably classify improvers from non-improvers better than chance. We then successfully cross-validated our H-based model on an independent fMRI dataset of 45 participants performing a different WM task. These results suggest that H can be used as an objective measure of cognitive state and have theoretical and practical implications for research on state-dependent learning potential.

## Introduction

A physical system whose large-scale behavior cannot be properly modelled as merely sum of its smaller components (i. e., a network with interactions between nodes) can be in different states based on whether the configuration is poised at minimum stability or not. At 'critical' state, the susceptibility of macro-scale configuration of the network to environmental input is maximum (Chialvo, 2004; Fraiman, Balenzuela, Foss, & Chialvo, 2009; Frette et al., 1996). For example, the network configuration of water molecules in a bucket of water at 0° C (critical state) can change drastically by shifting phase from liquid to solid or vice versa based on energy transfer between the bucket and its environment, but at -40° C (sub-critical state) same energy transfer will result in much less macro-scale change in the water molecules (i. e., the solid phase persists). One can model the brain as another such network, comprised of small-scale neuronal ensembles with short- and long-term interactions (phase-coupled electro-chemical activity) whose emergent large-scale activity give rise to cognitive functions (Chialvo, 2010; Cocchi, Gollo, Zalesky, & Breakspear, 2017; Fagerholm et al., 2015; Gisiger, 2001; He, 2014; Werner, 2010). Under this assumption, the temporal and spatial efficiency of information (energy) transfer between the nodes in the brain network, as well as between the brain and the environment, can also be in different states. There is evidence of self-organized criticality in the human brain during rest (de Arcangelis, Perrone-Capano, & Herrmann, 2006; Kitzbichler et al., 2009), with capability to transiently self-organize to other states (i. e., not close to criticality) depending on behavioral and cognitive demands (Arviv, Goldstein, & Shriki, 2015; Fagerholm et al., 2015; Hahn et al., 2017; Yu et al., 2017). We we will henceforth refer to these brain network states poised around criticality as 'cognitive states'

because of our assumption that cognitive functions are macro-scale manifestations of the brain network activities.

A common way of measuring large-scale critical dynamics in brain is estimating the scale-invariance (e. g. 1/f component of power spectral density function) of brain activity signals. Time scale-invariance of brain activity as measured by the Hurst exponent (*H*) of electrophysiological brain data (e. g. EEG, MEG, ECoG) or fMRI data has been shown to change based on cognitive states or developmental stages (Churchill et al., 2016; Goldberger et al., 2002; He, 2014; Kardan, Adam, et al., 2019). For example, in an EEG study by (Kardan, Adam, et al., 2019) it was found that when the brain is in an effortful state due to high working memory (WM) demand, its ability to adapt to other cognitive demands is diminished which exhibits itself in loss of criticality in brain networks, delineated by suppression of *H*. Therefore, under the assumption that a low H state indicates sub-criticality in brain, low level of scale-free brain activity could then indicate a lowered level of learning and plastic adaptation compared to the critical-state level (de Arcangelis & Herrmann, 2010), resulting in lack of further WM task improvements.

However, as promising as it may seem, scale-invariance (*H*) of brain signals has not been extensively investigated in studies of learning and working memory (WM) performance, nor have measures of scale-invariance been extensively compared to other network measures such as functional connectivity (Biazoli et al., 2017). While functional connectome-based models have been successful in predicting individual differences in an array of psychometric measures such as attention and intelligence (Rosenberg et al., 2016; Smith et al., 2015), there are no reported studies that directly compare their predictive

power for detecting change in performance (i. e., learning) to measures of scale-invariance. Such investigations are important because 1) beyond predictive power, functional connectome based models capitalize on statistical dependencies between brain regions and lack the same level of basic theoretical framework that exist for network criticality models (Hutchison et al., 2013), and 2) there is evidence of medium to large correspondence between scale invariance and global connectivity in human functional brain networks (Bassett, Meyer-Lindenberg, Achard, Duke, & Bullmore, 2006; Churchill et al., 2016; Ciuciu, Abry, & He, 2014), as well as correspondence in changes in the two measures under similar conditions (for example under distress, see (Churchill et al., 2015; Kardan, Reuter-Lorenz, et al., 2019), both of which point to a potential relationship between the two measures. Therefore, it is pertinent to both lines of research to investigate whether the learning of WM tasks is modulated by an individual's cognitive state, as indexed by *H*, and compare the predictive power of this broad-band signal characteristic in determining consequent task performance with that of functional connectome based models.

As such, in the current study we used *H* measured with fMRI data during learning phase of an audio-visual dual N-back (DNB) task and prior to secondary attempt at the task to predict improvement, or lack thereof, in task performance. Since an H-based model of brain state captures different scales of plasticity that are not task-specific phenomena (de Arcangelis & Herrmann, 2010) and is less sensitive to individual differences in WM capacity (Kardan, Adam, et al., 2019), it is plausible that *H* index of cognitive state during learning would predict change in performance on the DNB task more reliably than other models. Specifically, we propose that H-based model of cognitive state has higher prediction power for learning than using baseline task performance or fMRI functional

connectivity strength (both of which are likely to capitalize on WM capacity differences), and would generalize better to other WM tasks as well. We investigated this hypothesis in the current study, and our results provide evidence in support of utility of levels of brain activity scale-invariance as an objective measure of the individual's cognitive states.

## Methods

### Participants

68 participants (27 male, 41 female) aged between 18 and 40 years old (Mean = 24.3, SD = 5.6) were recruited from the University of Chicago and surrounding area through fliers and geotargeted facebook advertisements (30 White, 21 Asian, 13 Black, 4 Other). Twelve participants were excluded from analysis, resulting in n = 56 in the final sample. Two participants were excluded due to incomplete fMRI scanning data because of discomfort before the scanning session was finished. Two participants were excluded due to technical issues with audio/visual during a run. 5 participants were flagged for sleepiness during the data acquisition as indicated by their eye-movement behavior by two researchers on-site. Finally, five participants were excluded after primary data quality check using MRIQC (Esteban et al., 2017) due to excessive head movement and low tSNR (peak translation > 2 mm or rotation > 0.2 degree, tSNR < 50) during at least one of the scanning runs. All participants had self-reported normal or corrected-to-normal visual acuity and normal color vision. All participants gave informed consent and were compensated $35 for participation plus a potential bonus of $10. The participants were informed before the scanning session that if they "stay attentive and still" during scans they will get a $10 bonus. All participants included in the analysis had received the bonus during data acquisition.

**Experiment procedure**

Participants came to lab 45 minutes before the scanning session and were instructed by a research assistant on how to do an audio-visual dual n-back (DNB) task. Then, each participant performed one round of dual 2-back and one round of dual 3-back as practice, with each round containing 20+N trials (N = 2 or 3 for 2-back or 3-back respectively) to understand the task. If the performance was at or worse than chance level (sensitivity index $A' \leq 0.5$), additional rounds of practice were carried out until the participant understood the task and performance was better than chance. After the in-lab minimal practice, the scanning session started. In the fMRI scanner, after anatomical scans were collected, there were 3 functional runs starting with the first DNB run followed by a passive video watching run, and ending with the final DNB run. In the video run, participants were randomly assigned to passively watch one of two videos. The videos were mute and contained 10 minutes of either non-nature tourist attractions in Europe or outdoor nature scenes, and were equated for aesthetic preference. After the last run, participants were asked to give a preference rating (1-7 scale) for the video they watched to be included as a potential nuisance variable. In the DNB runs, the participants were instructed to perform the DNB task to the best of their ability.

**Audio-visual Dual N-back**

In an N-back task, participants are instructed to press a button if the current stimulus presented to them (visual or auditory) matches the stimulus N trials before. A dual N-Back (DNB) is a variant of n-back in which two simultaneous n-backs are presented to the participants in parallel. For this study, the two simultaneous n-backs involved an auditory n-back where the sound stimuli were numbers 1-9, and a spatial location n-back

where the position of a blue square in a 3*3 grid (see Fig. 2.1) had to be remembered. The paradigm is implemented in MATLAB and its code is publically available at https://enl.uchicago.edu/stimuli-software/. Participants pressed their right index finger, right middle finger, both fingers, or neither finger to respectively indicate position match, number match, both position and number match, and no match for each trial. Each trial was 3000 ms and the button press was allowed throughout the trial. Immediate feedback on position and number button presses were provided to the participant by change of color to red (incorrect press) or green (correct press) in the text on the bottom of the screen (see Figure 2.1).

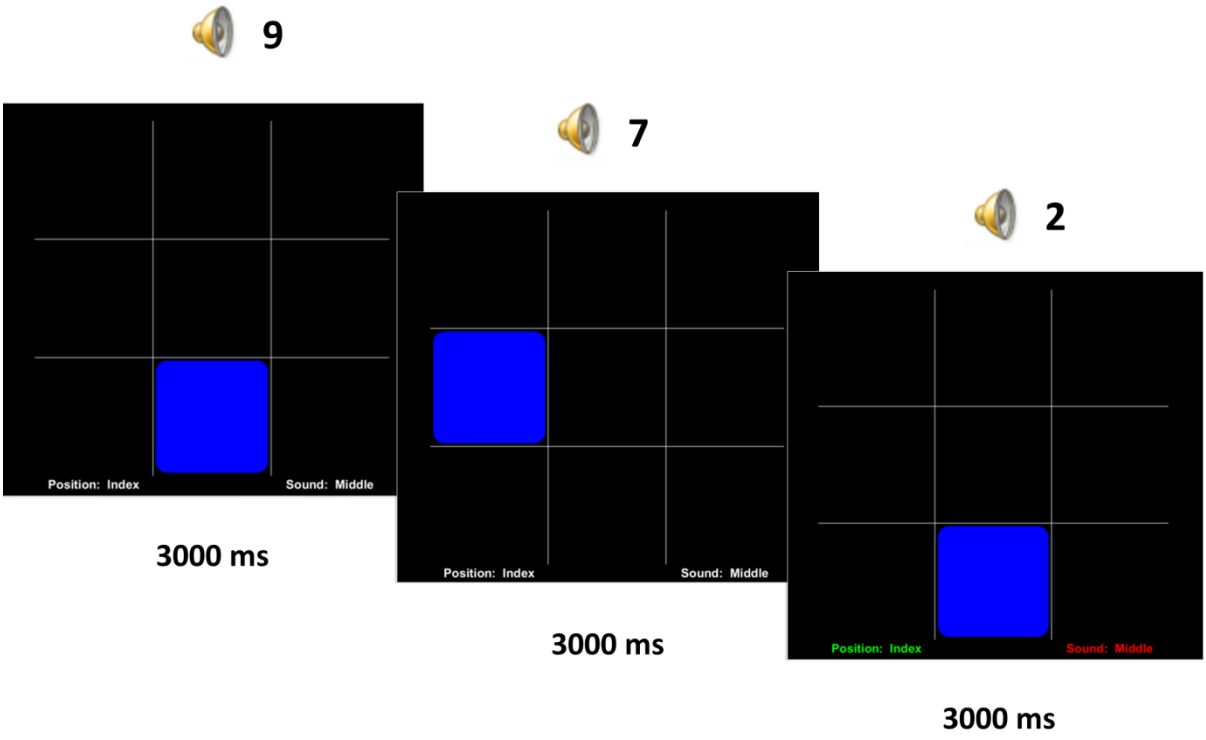


**Figure 2.1.** Audio-visual dual n-back (DNB) task paradigm. In this example for the first three trials in a dual 2-back round, the participant correctly pressed their index finger for a match between the current and 2-back position of blue square, but falsely pressed their middle finger when they should not have (2 does not match 9).

There were 6 rounds in each fMRI DNB run (four 2-back and two 3-back), each separated with a 10 sec countdown that indicated whether the next round is going to be a 2-back or a 3-back. Each round contained 20+N trials (N = 2 or 3), resulting in a total of 134 trials in each DNB fMRI run. We used sensitivity index A' (Stanislaw & Todorov, 1999) as the main measure of performance in DNB task, which is calculated as follows:

$$\text{Performance A'} = 0.5 + \frac{sign(Hit - FA) * [(Hit - FA)2 + abs(Hit - FA)]}{(4 * max(Hit, FA) - 4 * Hit * FA)}$$

Where Hit is the number of correct button presses and FA is the number of false alarms in a round of DNB. We averaged A' in all 6 rounds within each fMRI DNB run to index a participant's performance in the run. A' is very similar to other sensitivity indices such as d', but is more robust to non-normality of responses (Stanislaw & Todorov, 1999) , and A' = 0.5 delineates chance level of performance while A' = 1 shows perfect performance and A'<0.5 shows performance that is systematically worse than chance.

**fMRI data acquisition and preprocessing**

Images were acquired on a Philips Achieva 3.0 T scanner with a standard quadrature head coil. Functional T2* weighted images were acquired using an echo-planar sequence with 3.25 x 3.25 x 3.5 mm voxels with repetition time TR = 2000 ms. A T1-weighted gradient echo (MP-RAGE) anatomical image with 1 x 1 x 1 mm voxels was also acquired for each participant with the same FOV = 24 cm. Image preprocessing was completed using Advanced Normalization Tools (ANTs) (Avants et al., 2011). The processing included bias correction for magnetic field inhomogeneity in both functional and anatomical data (*N4* algorithm in ANTs), affine motion correction of functional data

using *antsMotionCorr* in ANTs, co-registering a participant's anatomical data to their averaged functional data in each run using symmetric normalization algorithm (*SyN*) in ANTs, warping anatomical images to ICBM-152 template, and finally applying the combined transformation matrices of the two previous steps on functional data. Denoising the data included nuisance regression of the first 3 principal components of motion parameters (PCs that account for > 85% of head movement parameters variance), linear detrending, and band-pass filtering to [0.01, 0.1] Hz for removing physiological noise and drift.

It is worth mentioning that a different version of pre-processing that additionally included slice-timing correction (AFNI 3dTshift) and spatial smoothing of functional data with 6 mm FWHM Gaussian kernel (AFNI 3dmerge), as well as nuisance regression of paradigm timing (DNB rounds 69 sec on, 10 sec off) was also carried out separately, but had virtually no effects on the results of our classification analysis (see *Feature selection and classification*). As such, further results are presented for the less pre-processed dataset.

**Detrended Fluctuations Analysis (DFA)**

The scale-free signal in fMRI data was estimated using Detrended Fluctuations Analysis (DFA), which is an efficient way to measure the Hurst exponent (H) in a way that is robust to signal non-stationary and low-frequency confounds (Churchill et al., 2016; Peng et al., 1995). The timeseries in a voxel over a run $x(t)$ of total length $T$ is first integrated and transformed into an unbounded random walk $y(t)$, where $y(t) = \sum_{i=1}^{t}(x(i) - x_{ave})$ ; $t = 1, \dots, T$, $x(i)$ is the $i$th data point in the timeseries and $x_{ave}$ is the average amplitude of the timeseries. Next, $y(t)$ is divided into windows of equal length n. A

least-square linear regression is fit to each subdivision of $y(t)$ with length $n$, with the fitted values denoted as $\hat{y}_n(t)$. Next we detrend the integrated timeseries $y(t)$ by subtracting the local trend, $\hat{y}_n(t)$ in each window. The root-mean-square magnitude of fluctuations on the detrended data $F(n)$ is then computed over a range of window sizes:

$$F(n) = \sqrt{\frac{1}{T}\sum_{t=1}^{T}[y(t) - \hat{y}_n(t)]^2}$$

Where $n$ = 50 TRs is maximum window size corresponding to 0.01 Hz minimum frequency, and $n$ = 3 TRs is minimum window size for fitting a line with a non-zero residual. Finally, the linear fit of $log(n)$ vs. $log(F(n))$ is calculated and the slope of this fitted line is used as the estimate of the degree of fractalness (H) for the voxel time-series $x(t)$. A slope of H = 0.5 indicates no long-range correlation in the signal (i. e., a random walk), while H values closer to 1 indicate greater power law scaling.

**Feature selection and classification**

We selected a subset of voxel regions of interest (ROI) and a subset of functional connections of interest (COI) from the final DNB fMRI run that were most relevant in distinguishing the improvers from non-improvers in the DNB task. No brain data from the first two runs (DNB1 and Video) was used in the ROI or COI selection, as they were planned to be used for classification. The selection of a subset of voxels for analysis (i. e., the ROI) and subset of connections for analysis (i. e., the COI) was done using these four steps (illustrated in Figure 2.2): 1) The sensitivity index A' was calculated for the two DNB runs using hits and false alarms in each run, and the fMRI data from run 3 (i. e., second DNB run)

was preprocessed (see *fMRI acquisition and pre-processing*). 2) DFA was applied to each voxel in the preprocessed fMRI time-series from run 3 to calculate the H for each voxel for each participant. Also, the data was downsampled to 392 regions by averaging voxels within each region of the CC-400 atlas (Craddock, James, Holtzheimer, Hu, & Mayberg, 2012), and the Pearson correlation between every pair of regions was calculated and squared. The downsampling was done to reduce the number of pairwise connections to Choose(392,2) = 76636, rather than ~2 billion pairs from the non-down sampled voxel space. The CC-400 atlas was used because it provided 76K pairwise connections, which is in the same order of magnitude as the number of voxels and thus keeps the H and $r^2$ matrices used for selecting ROI and COI comparable in size. 3) We then regressed out the baseline performance ($A'_0$) from the performance change variable ($\Delta A' = A' - A'_0$) and used the residuals as the adjusted change in performance. This adj. $\Delta A'$ vector was correlated with 200 bootstraps (resample with replacement) of the matrix of H values and C values to find voxels or connections that correlated with the adj. $\Delta A'$ above a threshold of 0.25 Pearson correlation. Although there is not a clear consensus on choosing the threshold, the classification accuracies were very robust to the choice of correlation threshold in the typical range of 0.2 to 0.3 despite slight differences in ROI and COI sparseness. Thus we chose the upper bound for a 'small' association size (r = 0.25) according to (Kirk, 2012) as the threshold. 4) Voxels and connections that passed this threshold in more than half of the bootstraps were assigned as being a member of the analysis ROI and COI, respectively. Figure 2.4 shows these voxels (Figure 2.4A) and connections (Figure 2.4B) which are comprised of 5409 voxels (~8.5%) and 2747 pairwise connections (~3.6%), respectively. The ROI voxels fall mainly within frontal and temporal lobes and the COI connections

mainly involve temporal and frontal lobes, as well as cerebellum. The full list of brain structures with some overlap with the Hurst ROI and the $r^2$ COI are presented in supplementary Tables S1.1 and S1.2. Finally, the H and functional connectivity strength in runs 1 and 2 were averaged over these ROI and COI for each participant and used to classify the improvers and non-improvers in a linear discriminant (LD) classification implemented in MATLAB with leave-one-participant-out cross-validation. A distribution of classification accuracies was constructed by bootstrapping (1000 resamples with replacement) the participants with intact class labels (improver vs. non-improver). Predictive power of each feature (i. e., $H_{DNB1}$, $H_{Vid}$, $Conn_{DNB1}$, or $Conn_{Vid}$) was then tested against a null distribution with permuted class labels to test for statistical significance of classifications.

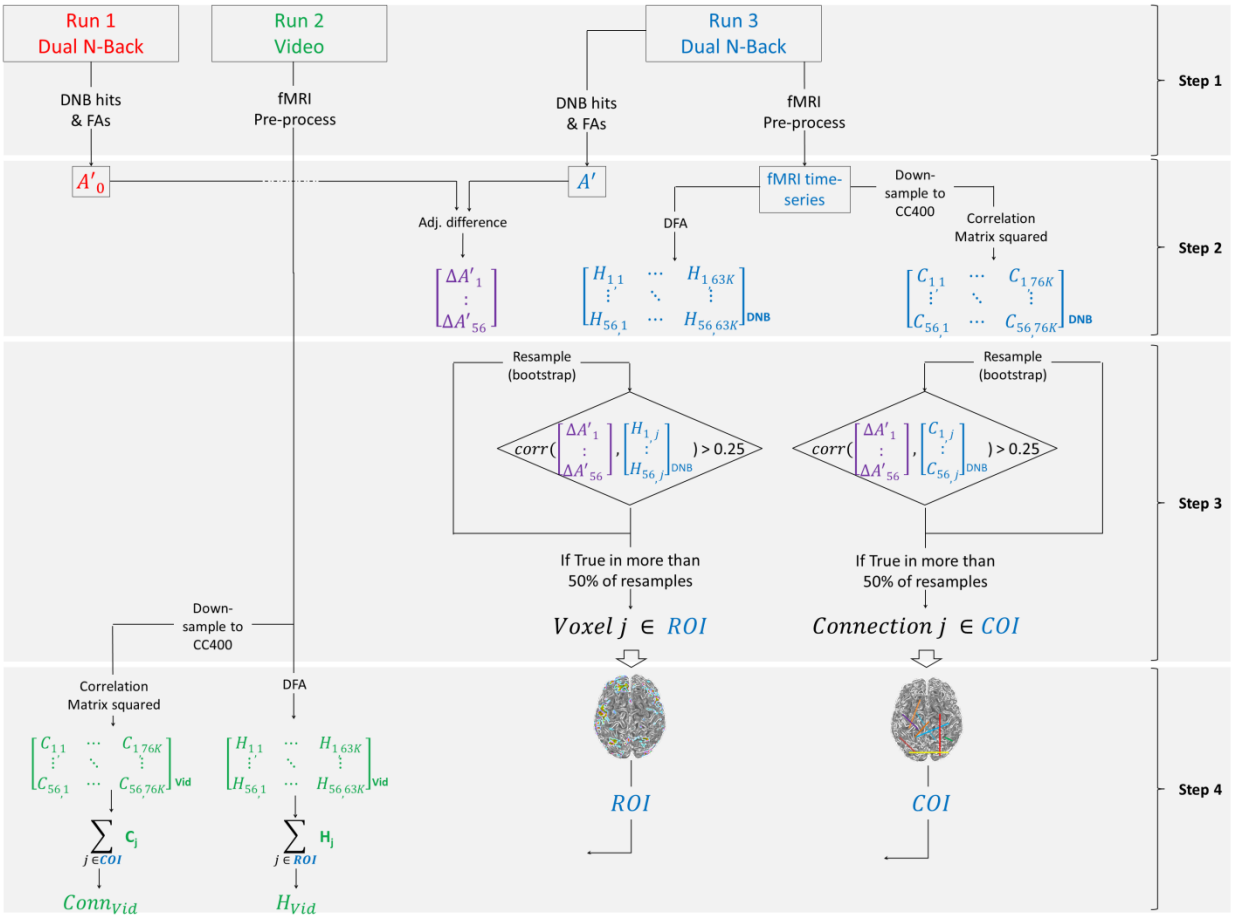


**Figure 2.2.** Steps in selection of voxels (ROI) and pairwise functional connections (COI) that enhance the distinction in H and functional connectivity between task improvers and non-improvers based on run 3 of the fMRI session. The H and $r^2$ from prior runs (DNB1 and Video) are then averaged in these selected ROI and COI for each participant, denoted as $H_{Vid}$ or $H_{DNB1}$ and $Conn_{Vid}$ or $Conn_{DNB1}$ respectively, and used for classification in the DNB data. The same ROI and COI are also later used in the independent fMRI dataset of word completion task.

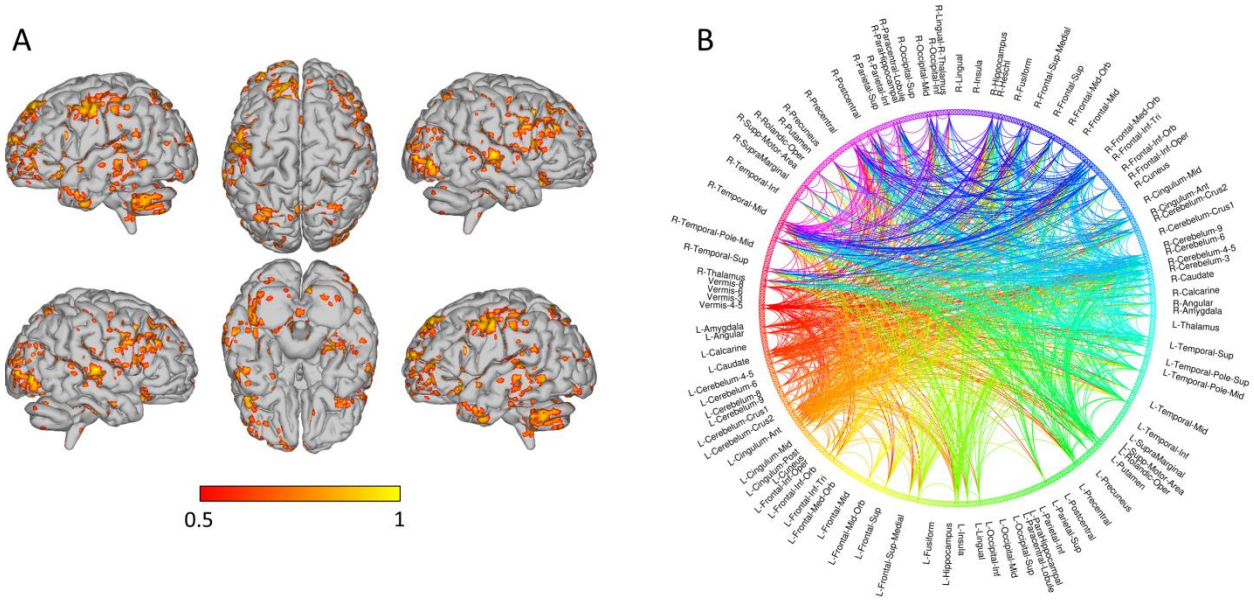


**Figure 2.3.** The selected ROI (A) and COI (B) are illustrated here. A. The main clusters of the Hurst ROI are located in the frontal and temporal lobes. The complete list of anatomical regions overlapping with the ROI voxels are in supplementary Table S2.1. B. The nodes with most connections in the $r^2$ COI involve temporal and frontal regions, as well as cerebellum. The complete list of anatomical regions seeding connections in the COI can be found in supplementary Table S2.2.

**Independent sample cross validation**

We also used the average H over the same ROI from the DNB experiment dataset to predict improvers and non-improvers in an independent sample of 45 subjects performing a completely different WM task (word completion task). The dataset was provided by Choe et al. 2019 (unpublished results) and consists of 6 fMRI runs for 45 participants aged between 18-40 who performed a math and word Choose-and-Solve Task (CAST) for 6 minutes in every run. This task involves choosing to solve math equation completion and word completion tasks and is originally designed for detecting math anxiety and math avoidance behavior. The participants performed the CAST in 6 runs in fMRI scanner which provided us with a different learning paradigm to cross-validate the *H*-based classification model used for DNB. The questions were designated as having a 1-7 difficulty level based

on a previous study (Choe et al. 2019 unpublished behavioral study). The performance of participants in CAST was quantified as their accuracy*difficulty level of questions they solved, since the question difficulty was adaptive in a manner that two correct answers in a row would result in an increase in difficulty and one wrong answer would result in decrease in question difficulty. Since the number of trials where difficult math questions (with higher reward) were chosen over easy math questions (with lower reward) was very sparse across participants, performance was quantified only over word-completion trials. In word completion trials, participants see words with omitted letters replaced by ~ and □. The participant has to quickly choose (< 2000 msec) the correct letter that should be in the square (i. e., □). For example, for E~□DE~CE, the correct choice is letter 'I' (the word is 'evidence'). In this dataset, the fMRI acquisition parameters were identical to our DNB dataset and we pre-processed and calculated *H* values identically to the DNB dataset. The improvers and non-improvers were again labeled by a median split on change in performance between run 6 compared to run 1, adjusted for performance in run 1. The improvers had an average increase of 23% on their task performance compared to – decrease of -16% for non-improvers.

## Results

### Experiment 1: DNB task performance

There was an average improvement of 0.045 in A' (5.5%) from DNB1 to DNB2 (Figure 2.4 left), showing learning in overall sample. Linear regression of ΔA' on video type, preference rating for the video, and baseline DNB performance ($A'_0$) showed no relationship between change in performance and video type (t = 0.403, p = 0.688) or preference rating (t = -0.870,

p = 0.388), but a significant relationship between baseline performance and change in performance (t = -2.248, p = 0.029). Therefore, we collapsed the participants on the video types but regressed $A'_0$ out of ΔA' before splitting the participants to improvers and non-improvers (Figure 2.4 right).

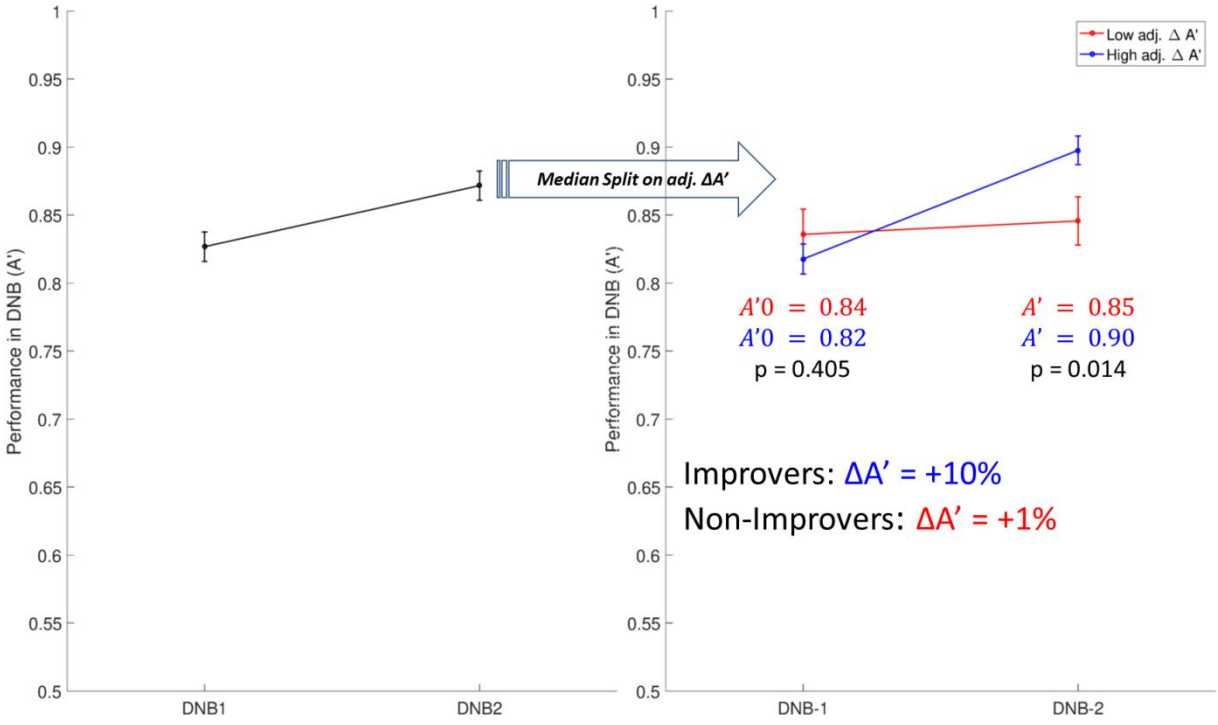


**Figure 2.4.** Performance in DNB task in all participants (left) and separated by change in performance for improvers and non-improvers (right). Errorbars show ±SE.

## Experiment 1 fMRI results: Predictive power of scale-invariance versus connectivity strength

The classification of improvers vs. non-improvers was successful using either average *H* in the ROI during the baseline DNB run (i. e., $H_{DNB1}$) or average H in the ROI during the passive video viewing run (i. e., $H_{Vid}$), with both having medium prediction accuracies of 64% and significantly better than the null classification distribution (p =

0.025 and p = 0.005 for $H_{DNB1}$ and $H_{Vid}$, respectively). The distribution for all classification bootstraps and their respective confusion matrices are shown in Figure 2.5 panels A and B. As mentioned before, to compare these accuracies with predictive power of functional connectivity, we applied identical bootstrap samples in a leave-one-out LD classification trained on the average $r^2$ values in the COI during the baseline DNB ($Conn_{DNB1}$) or average $r^2$ in the COI during the passive viewing run ($Conn_{Vid}$). As shown in Figure 2.5 panel A, neither $Conn_{DNB1}$ or $Conn_{Vid}$ predicted improvers from non-improvers significantly better than the null model, with respective accuracies of 53% and 57%.[5]

Another approach to control for baseline DNB performance differences, rather than adjusting ΔA' for it, is to only use the fMRI data from the video run (i. e., $H_{Vid}$ or $Conn_{Vid}$) to predict improvers and non-improvers regardless of their baseline performance. In order to make sure a simpler model using only the baseline behavioral performance (i. e., performance in DNB1 run, $A'_0$) would not result in similar classification accuracy, a second classification was done where the median split was done on ΔA' non-adjusted for baseline performance. We repeated the classification procedure using the $H_{Vid}$, $Conn_{Vid}$, or the baseline performance to distinguish the new split of improvers and non-improvers that does not adjust for baseline performance. The results, shown in Figure 2.5 panels C and D show similar prediction accuracy of 64% (p = 0.025) for $H_{Vid}$, while neither $Conn_{Vid}$ nor baseline performance have classification accuracies better than chance (57% and 58%, respectively). Additionally, we used all three variables ($A'_0$, $H_{Vid}$, and $Conn_{Vid}$) and their interactions for classification and left each variable out to see the drop in prediction

[5] Separate analysis of negative and positive functional connectivity values (rather than $r^2$) resulted in slightly worse performance for the connectivity-based classifications.

accuracy. This analysis showed that $Conn_{Vid}$ was completely redundant to the full model (i.e., no accuracy drop absent of $Conn_{Vid}$), and the best classification model was one with combined $H_{Vid}$ and $A'_0$, which performed at 70% accuracy (Figure 2.5 panels C and D, best model).

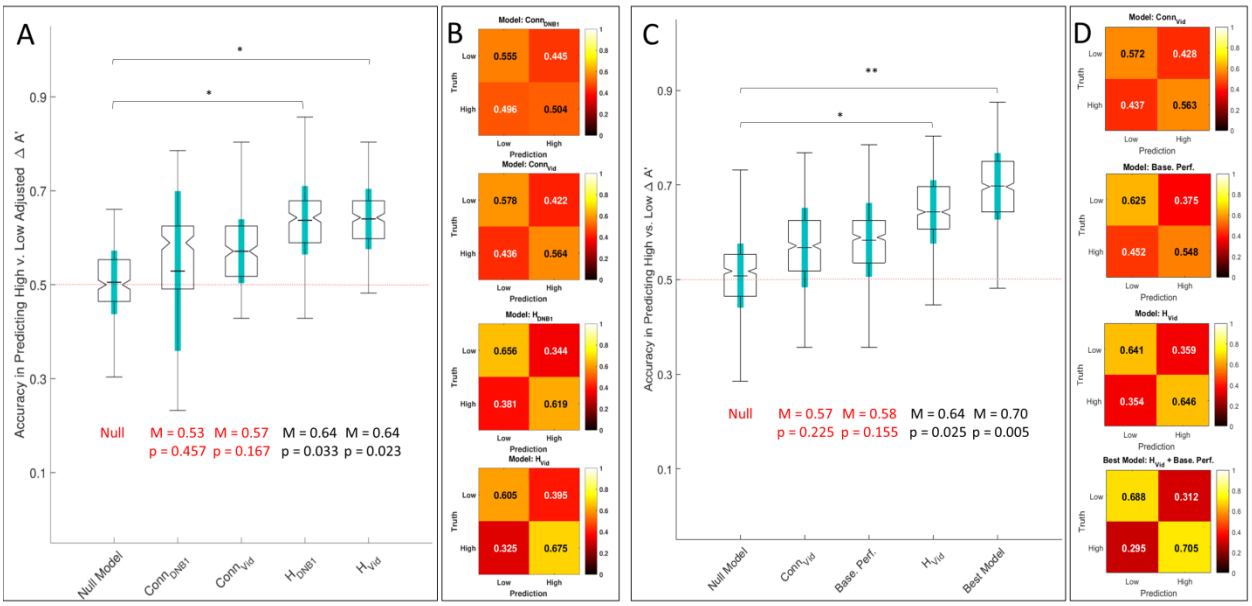


**Figure 2.5.** Classification accuracy distributions and confusion matrices. A. The classes are based on median split of adj. ΔA'. The p values compare the null model distribution with model congaing the variable indicated on the x axis. M shows mean of the distribution (so do black horizontal ticks inside the boxes), notch in the boxes show medians of distributions, and thick light blue vertical lines show the SD of distributions around the means. The boxes show ±1 quantile around the median and whiskers show range of the distribution. All stats reported include all 1000 bootstrap sample accuracies, but some outlier points are not included in the visualization of graphs.

Next, we plotted the average H in whole brain and also within the selected ROI across the three runs of the experiment for improvers and non-improvers (Figure 2.6 panels A and B, respectively) to investigate the group differences that lead to successful classification. Even before ROI specification, there is an indication of global higher *H* overall brain averaged over all runs for improvers compared to non-improvers, although the effect

is trending ($t = 1.99$, $p = 0.052$). This distinction considerably increases with ROI selection (Figure 2.6B) which allows for successful classification. Additionally, both global and ROI *H* are higher during the video run compared to the DNB runs ($t = 4.19$, $p < 0.001$ for global *H* and $t = 4.12$, $p < 0.001$ for ROI *H*). This replicates previous findings about global *H* suppression in fMRI and EEG brain signals tracking higher cognitive effort and level of task difficulty (Churchill et al., 2016; Kardan, Adam, et al., 2019). Figure 2.6 panel B also delineates that ROI selection using the third run (DNB2) successfully increased the *H* distinction between the improvers and non-improvers in a manner that generalizes to runs prior to it. In comparison, the distinction created by COI selection for functional connectivity strength did not generalize to previous runs (Figure 2.6 panels C and D).

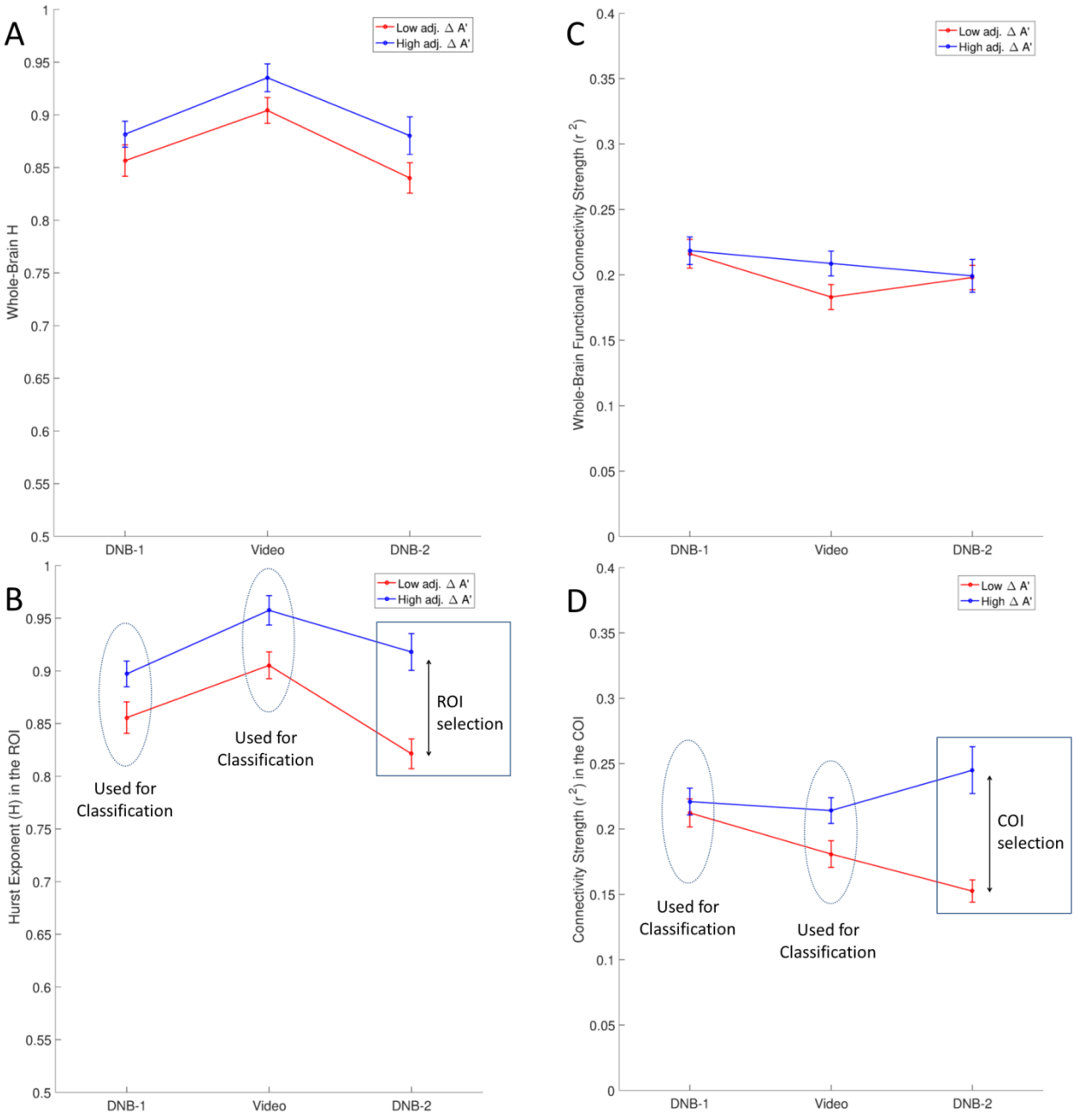


**Figure 2.6.** The average H (left panels) and average r2 (right panels) for improvers and non-improvers. The H values are averaged over whole brain in A and over the ROI in C. The r2 values are averaged over all pairwise connections in B and over the COI in D.

**Experiment 2: Independent sample cross-validation (word completion task)**

We used fMRI data from an independent sample of 45 participants from Choe et al., [unpublished study] to classify task improvers from non-improvers in a different working memory task, the word completion task (as part of a Choose-and-Solve Task (CAST), see *methods*). The performance levels of participants are shown in Figure 2.7, and panel B shows the performance separately for the two groups of improvers and non-improvers. The two groups were made similarly to the DNB dataset, where a median split in change in performance between the last and the first run and adjusted for the baseline performance (i. e., adj. *Δ Performance*) determined the dichotomy for classification. The average *H* in the pre-defined ROI from our DNB dataset was calculated for each participant, and the mean values for each group (improvers and noon-improvers) are plotted in Figure 2.7 panel C. We used the ROI *H* in earlier runs (1, 2, and 3) to classify the improvers and non-improvers similar to DNB dataset, and the results of LD classification with leave-one-out cross-validation procedure are shown in Figure 2.7D. Using the *H* from the first half of the session (first 3 runs out of 6) was sufficient for the classifier to successfully distinguish improvers from non-improvers above chance (63% accuracy, $p = 0.011$ compared to null distribution). Importantly, there was no difference in reaction time to attention check trials between the improvers and non-improvers (965 ms for non-improvers vs. 956 ms for improvers, $t = 0.135$, $p = 0.893$) in this dataset, ruling out any potential differences in level of task engagement between the two groups.

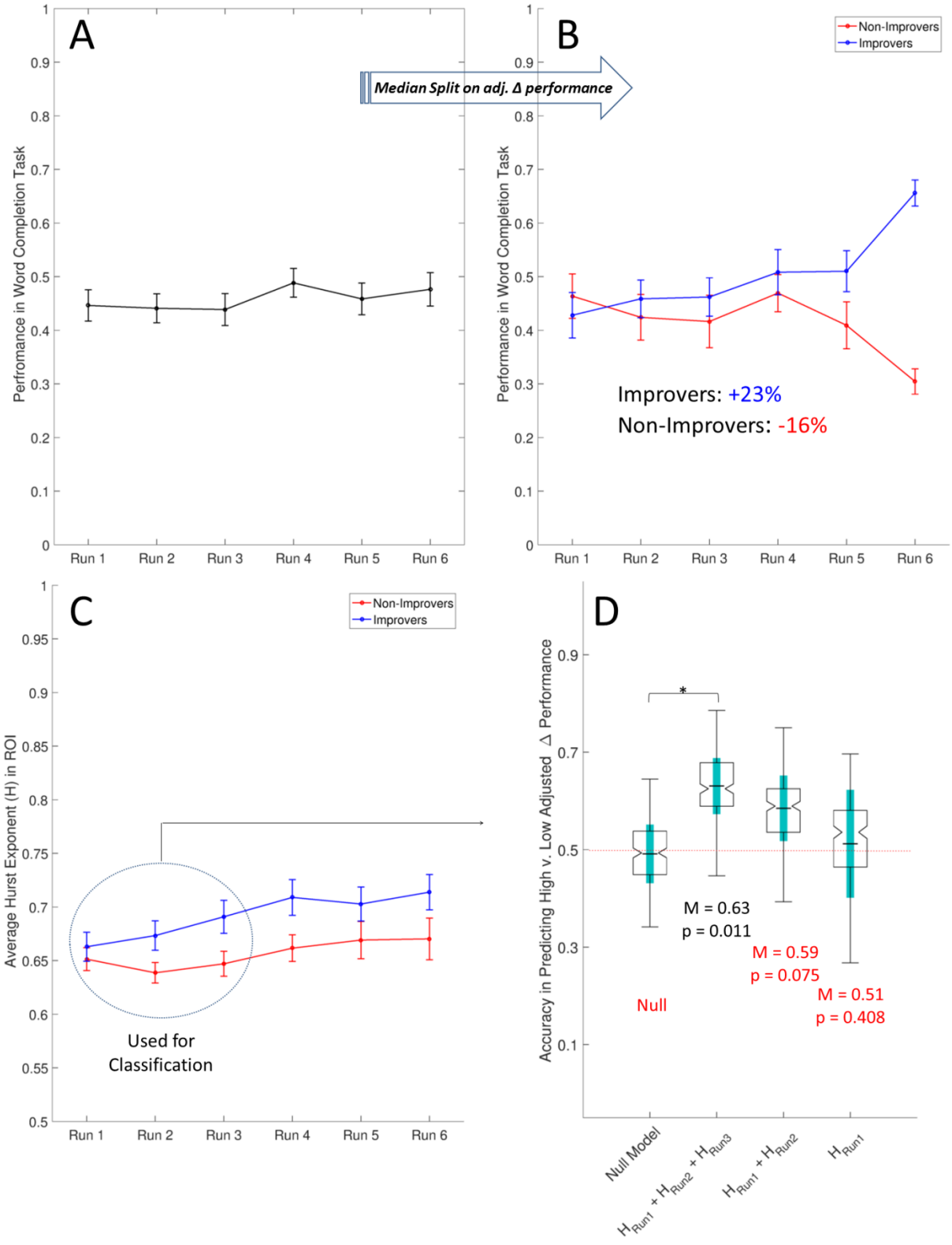


**Figure 2.7.** Behavioral performance in word completion task across runs (A), and separated by improvers vs. non-improvers groups (B). The *H* in the pre-defined ROI from

[**Figure 2.7. continued]** the DNB experiment over all runs are shown in panel (C). Panel (D) shows classification accuracy boxplots of LD classifier with leave-one-participant-out cross-validation using the variable(s) indicated on the x axis. The p values compare each model with the null distribution, and thick vertical green lines indicate SD around the mean of distributions.

## Discussion

In the current study we found scale-free dynamics of the BOLD signal during the process of learning difficult cognitive tasks (that placed demands on WM) to be a reliable signal for predicting cognitive task improvement. We compared our H-based model's performance with that of a functional connectome based model with similar feature selection steps and found the H-based model to have superior predictive power. We also cross-validated our model for different datasets with different WM tasks (audio-visual DNB vs. word completion task). The H-based model successfully predicted task improvers and non-improvers, who had similar baseline task performance, in both datasets. Together, these findings provide evidence for utilizing scale-free dynamics of brain activity as an objective measure to determine an individual's cognitive state during learning (i. e., learning potential) which enables forecast of future performance.

Under the assumption that the observed scale-invariance differences in the current study delineate cognitive states of criticality in brain networks (see (Muñoz, 2018) for other concepts in biology also termed as criticality and (von Wegner et al., 2018) for other interpretations of scale-free brain activity), one can interpret the higher *H* state of the brain for an individual as indicative of them being more receptive to the input received during learning the task and thus improving their performance more readily. This follows research on neural networks showing criticality optimizes a number of computationally advantageous properties (Beggs John M, 2008; Shew & Plenz, 2013), such as the dynamic

range of the network (Gautam, Hoang, McClanahan, Grady, & Shew, 2015; Kinouchi & Copelli, 2006), and active information storage and transfer (Boedecker, Obst, Lizier, Mayer, & Asada, 2012; Shriki et al., 2013; Shriki & Yellin, 2016; Tanaka, Kaneko, & Aoyagi, 2008). This interpretation of our results is plausible because improving on most complex working memory and attention tasks requires a degree of switching between sub-tasks and changes in locus of attention (Awh & Jonides, 2001; Ikkai & Curtis, 2011), both of which depend on large-scale sensitivity of neuronal ensembles to the dynamics of received input/stimulus and efficiency of information transfer and storage within the brain network. As such, learning is likely to be facilitated when the brain is closer to its self-organized critical state of 'rest' (He, 2011; Kitzbichler et al., 2009; Proekt, Banavar, Maritan, & Pfaff, 2012) due to temporal and spatial efficiency of information transfer between nodes of the brain networks, as well as between environment and the brain. On the other hand, a sub-critical state, as indicated by lower *H*, might reflect a loss of sensitivity to environmental signal as a trade-off for gaining specificity (Gollo, 2017) which is sub-optimal for WM task learning, although it may be beneficial for other behaviors that are less dependent on active input-output mapping (Gollo, 2017; Latham & Nirenberg, 2004).

In a recent article about the burgeoning field of environmental neuroscience (Berman, Kardan, Kotabe, Nusbaum, & London, 2019), the authors theorize that the degree of susceptibility of an individual to environmental stimulations could modulate the level of beneficial or detrimental effects from positive or negative environments. However, the main mechanisms for individual differences in environmental susceptibility are proposed to be genetic and epi-genetic factors. Future studies should investigate whether individual differences in brain network criticality as measured by *H* could be another factor of

susceptibility to be considered in environmental neuroscience theories and other research related to human-environment interactions. Regarding application, (Kardan, Adam, et al., 2019) proposed that measuring the suppression of scale-free brain activity can hypothetically serve as a robust neuro-feedback when devising educational interventions, as *H* in both BOLD (Churchill et al., 2016) and EEG activity (Kardan, Adam, et al., 2019) are sensitive to cognitive effort rather than to the specific nature of the procedure or task performance. In contrast, other bio-marker candidates such as narrow-band EEG oscillations and eye-tracking features are often confounded with individual differences in WM capacity or characteristics of the task at hand (Adam et al., 2018; Kardan, Berman, Yourganov, Schmidt, & Henderson, 2015; Kardan, Henderson, Yourganov, & Berman, 2016). Our current results support that such proposal is tenable and further pave the way for applications of H-based models for learning and skill acquisition. Last but not least, our results indicate that recent research on links between scale-free dynamics and graph-theoretical measures of functional connectivity (Churchill et al., 2015; Ciuciu et al., 2014) should be expanded as they could provide new insights on a general theoretical framework for how cross-regional interactions emerge in the brain.

## References


Adam, K. C. S., Robison, M. K., & Vogel, E. K. (2018). Contralateral Delay Activity Tracks Fluctuations in Working Memory Performance. *Journal of Cognitive Neuroscience*, *30*(9), 1229–1240. https://doi.org/10.1162/jocn_a_01233

Adam, K. C. S., Vogel, E. K., & Awh, E. (2017). Clear evidence for item limits in visual working memory. *Cognitive Psychology*, *97*, 79–97. https://doi.org/10.1016/j.cogpsych.2017.07.001

Alvarez, G. A., & Cavanagh, P. (2004). The Capacity of Visual Short-Term Memory is Set Both by Visual Information Load and by Number of Objects. *Psychological Science*, *15*(2), 106–111. https://doi.org/10.1111/j.0963-7214.2004.01502006.x

Arviv, O., Goldstein, A., & Shriki, O. (2015). Near-Critical Dynamics in Stimulus-Evoked Activity of the Human Brain and Its Relation to Spontaneous Resting-State Activity. *Journal of Neuroscience*, *35*(41), 13927–13942. https://doi.org/10.1523/JNEUROSCI.0477-15.2015

Avants, B. B., Tustison, N. J., Song, G., Cook, P. A., Klein, A., & Gee, J. C. (2011). A reproducible evaluation of ANTs similarity metric performance in brain image registration. *NeuroImage*, *54*(3), 2033–2044. https://doi.org/10.1016/j.neuroimage.2010.09.025

Awh, E., & Jonides, J. (2001). Overlapping mechanisms of attention and spatial working memory. *Trends in Cognitive Sciences*, *5*(3), 119–126. https://doi.org/10.1016/S1364-6613(00)01593-X

Barnes, A., Bullmore, E. T., & Suckling, J. (2009). Endogenous Human Brain Dynamics Recover Slowly Following Cognitive Effort. *PLOS ONE*, *4*(8), e6626. https://doi.org/10.1371/journal.pone.0006626

Bassett, D. S., Meyer-Lindenberg, A., Achard, S., Duke, T., & Bullmore, E. (2006). Adaptive reconfiguration of fractal small-world human brain functional networks. *Proceedings of the National Academy of Sciences*, *103*(51), 19518–19523. https://doi.org/10.1073/pnas.0606005103

Beggs John M. (2008). The criticality hypothesis: how local cortical networks might optimize information processing. *Philosophical Transactions of the Royal Society A: Mathematical, Physical and Engineering Sciences*, *366*(1864), 329–343. https://doi.org/10.1098/rsta.2007.2092

Berman, M. G., Kardan, O., Kotabe, H. P., Nusbaum, H. C., & London, S. E. (2019). The promise of environmental neuroscience. *Nature Human Behaviour*, 1. https://doi.org/10.1038/s41562-019-0577-7

Biazoli, C. E. J., Salum, G. A., Pan, P. M., Zugman, A., Amaro, E. J., Rohde, L. A., … Sato, J. R. (2017). Commentary: Functional connectome fingerprint: identifying individuals

using patterns of brain connectivity. *Frontiers in Human Neuroscience*, *11*. https://doi.org/10.3389/fnhum.2017.00047

Boedecker, J., Obst, O., Lizier, J. T., Mayer, N. M., & Asada, M. (2012). Information processing in echo state networks at the edge of chaos. *Theory in Biosciences*, *131*(3), 205–213. https://doi.org/10.1007/s12064-011-0146-8

Bonner, S. E., & Sprinkle, G. B. (2002). The effects of monetary incentives on effort and task performance: theories, evidence, and a framework for research. *Accounting, Organizations and Society*, *27*(4), 303–345. https://doi.org/10.1016/S0361-3682(01)00052-6

Botvinick, M., & Braver, T. (2015). Motivation and Cognitive Control: From Behavior to Neural Mechanism. *Annual Review of Psychology*, *66*(1), 83–113. https://doi.org/10.1146/annurev-psych-010814-015044

Brainard, D. H. (1997). The Psychophysics Toolbox. *Spatial Vision*, *10*(4), 433–436. https://doi.org/10.1163/156856897X00357

Chialvo, D. R. (2004). Critical brain networks. *Physica A: Statistical Mechanics and Its Applications*, *340*(4), 756–765. https://doi.org/10.1016/j.physa.2004.05.064

Chialvo, D. R. (2010). Emergent complex neural dynamics. *Nature Physics*, *6*(10), 744–750. https://doi.org/10.1038/nphys1803

Churchill, N. W., Cimprich, B., Askren, M. K., Reuter-Lorenz, P. A., Jung, M. S., Peltier, S., & Berman, M. G. (2015). Scale-free brain dynamics under physical and psychological distress: Pre-treatment effects in women diagnosed with breast cancer. *Human Brain Mapping*, *36*(3), 1077–1092. https://doi.org/10.1002/hbm.22687

Churchill, N. W., Spring, R., Grady, C., Cimprich, B., Askren, M. K., Reuter-Lorenz, P. A., … Berman, M. G. (2016). The suppression of scale-free fMRI brain dynamics across three different sources of effort: aging, task novelty and task difficulty. *Scientific Reports*, *6*, 30895. https://doi.org/10.1038/srep30895

Ciuciu, P., Abry, P., & He, B. J. (2014). Interplay between functional connectivity and scale-free dynamics in intrinsic fMRI networks. *NeuroImage*, *95*, 248–263. https://doi.org/10.1016/j.neuroimage.2014.03.047

Cocchi, L., Gollo, L. L., Zalesky, A., & Breakspear, M. (2017). Criticality in the brain: A synthesis of neurobiology, models and cognition. *Progress in Neurobiology*, *158*, 132–152. https://doi.org/10.1016/j.pneurobio.2017.07.002

Craddock, R. C., James, G. A., Holtzheimer, P. E., Hu, X. P., & Mayberg, H. S. (2012). A whole brain fMRI atlas generated via spatially constrained spectral clustering. *Human Brain Mapping*, *33*(8), 1914–1928. https://doi.org/10.1002/hbm.21333

de Arcangelis, L., & Herrmann, H. J. (2010). Learning as a phenomenon occurring in a critical state. *Proceedings of the National Academy of Sciences*, *107*(9), 3977–3981. https://doi.org/10.1073/pnas.0912289107

de Arcangelis, L., Perrone-Capano, C., & Herrmann, H. J. (2006). Self-Organized Criticality Model for Brain Plasticity. *Physical Review Letters*, *96*(2), 028107. https://doi.org/10.1103/PhysRevLett.96.028107

Delorme, A., & Makeig, S. (2004). EEGLAB: an open source toolbox for analysis of single-trial EEG dynamics including independent component analysis. *Journal of Neuroscience Methods*, *134*(1), 9–21. https://doi.org/10.1016/j.jneumeth.2003.10.009

Engel, A. K., & Fries, P. (2010). Beta-band oscillations—signalling the status quo? *Current Opinion in Neurobiology*, *20*(2), 156–165. https://doi.org/10.1016/j.conb.2010.02.015

Esteban, O., Birman, D., Schaer, M., Koyejo, O. O., Poldrack, R. A., & Gorgolewski, K. J. (2017). MRIQC: Advancing the automatic prediction of image quality in MRI from unseen sites. *PLOS ONE*, *12*(9), e0184661. https://doi.org/10.1371/journal.pone.0184661

Fagerholm, E. D., Lorenz, R., Scott, G., Dinov, M., Hellyer, P. J., Mirzaei, N., … Leech, R. (2015). Cascades and Cognitive State: Focused Attention Incurs Subcritical Dynamics. *Journal of Neuroscience*, *35*(11), 4626–4634. https://doi.org/10.1523/JNEUROSCI.3694-14.2015

Foster, J. J., & Awh, E. (2019). The role of alpha oscillations in spatial attention: limited evidence for a suppression account. *Current Opinion in Psychology*, *29*, 34–40. https://doi.org/10.1016/j.copsyc.2018.11.001

Fraiman, D., Balenzuela, P., Foss, J., & Chialvo, D. R. (2009). Ising-like dynamics in large-scale functional brain networks. *Physical Review E*, *79*(6), 061922. https://doi.org/10.1103/PhysRevE.79.061922

Frette, V., Christensen, K., Malthe-Sørenssen, A., Feder, J., Jøssang, T., & Meakin, P. (1996). Avalanche dynamics in a pile of rice. *Nature*, *379*(6560), 49. https://doi.org/10.1038/379049a0

Fukuda, K., Awh, E., & Vogel, E. K. (2010). Discrete capacity limits in visual working memory. *Current Opinion in Neurobiology*, *20*(2), 177–182. https://doi.org/10.1016/j.conb.2010.03.005

Fukuda, K., Kang, M.-S., & Woodman, G. F. (2016). Distinct neural mechanisms for spatially lateralized and spatially global visual working memory representations. *Journal of Neurophysiology*, *116*(4), 1715–1727. https://doi.org/10.1152/jn.00991.2015

Fukuda, K., Mance, I., & Vogel, E. K. (2015). α Power Modulation and Event-Related Slow Wave Provide Dissociable Correlates of Visual Working Memory. *Journal of Neuroscience*, *35*(41), 14009–14016. https://doi.org/10.1523/JNEUROSCI.5003-14.2015

Garbarino, E. C., & Edell, J. A. (1997). Cognitive Effort, Affect, and Choice. *Journal of Consumer Research*, *24*(2), 147–158. https://doi.org/10.1086/209500

Gautam, S. H., Hoang, T. T., McClanahan, K., Grady, S. K., & Shew, W. L. (2015). Maximizing Sensory Dynamic Range by Tuning the Cortical State to Criticality. *PLOS Computational Biology*, *11*(12), e1004576. https://doi.org/10.1371/journal.pcbi.1004576

Gisiger, T. (2001). Scale invariance in biology: coincidence or footprint of a universal mechanism? *Biological Reviews*, *76*(2), 161–209. https://doi.org/10.1017/S1464793101005607

Goldberger, A. L., Amaral, L. A. N., Hausdorff, J. M., Ivanov, P. C., Peng, C.-K., & Stanley, H. E. (2002). Fractal dynamics in physiology: Alterations with disease and aging. *Proceedings of the National Academy of Sciences*, *99*(suppl 1), 2466–2472. https://doi.org/10.1073/pnas.012579499

Gollo, L. L. (2017). Coexistence of critical sensitivity and subcritical specificity can yield optimal population coding. *Journal of The Royal Society Interface*, *14*(134), 20170207. https://doi.org/10.1098/rsif.2017.0207

Hahn, G., Ponce-Alvarez, A., Monier, C., Benvenuti, G., Kumar, A., Chavane, F., … Frégnac, Y. (2017). Spontaneous cortical activity is transiently poised close to criticality. *PLOS Computational Biology*, *13*(5), e1005543. https://doi.org/10.1371/journal.pcbi.1005543

He, B. J. (2011). Scale-Free Properties of the Functional Magnetic Resonance Imaging Signal during Rest and Task. *Journal of Neuroscience*, *31*(39), 13786–13795. https://doi.org/10.1523/JNEUROSCI.2111-11.2011

He, B. J. (2014). Scale-free brain activity: past, present, and future. *Trends in Cognitive Sciences*, *18*(9), 480–487. https://doi.org/10.1016/j.tics.2014.04.003

Heitz, R. P., Schrock, J. C., Payne, T. W., & Engle, R. W. (2008). Effects of incentive on working memory capacity: behavioral and pupillometric data. *Psychophysiology*, *45*(1), 119–129.

Hotelling, H. (1936). Relations Between Two Sets of Variates. *Biometrika*, *28*(3/4), 321–377. https://doi.org/10.2307/2333955

Hutchison, R. M., Womelsdorf, T., Allen, E. A., Bandettini, P. A., Calhoun, V. D., Corbetta, M., … Chang, C. (2013). Dynamic functional connectivity: Promise, issues, and

interpretations. *NeuroImage*, *80*. https://doi.org/10.1016/j.neuroimage.2013.05.079

Ikkai, A., & Curtis, C. E. (2011). Common neural mechanisms supporting spatial working memory, attention and motor intention. *Neuropsychologia*, *49*(6), 1428–1434. https://doi.org/10.1016/j.neuropsychologia.2010.12.020

Jaffard, S., Lashermes, B., & Abry, P. (2007). Wavelet Leaders in Multifractal Analysis. In T. Qian, M. I. Vai, & Y. Xu (Eds.), *Wavelet Analysis and Applications* (pp. 201–246). https://doi.org/10.1007/978-3-7643-7778-6_17

Kardan, O., Adam, K. C. S., Mance, I., Churchill, N. W., Vogel, E. K., & Berman, M. (2019). *Distinguishing cognitive effort and working memory load using scale-invariance and alpha suppression in EEG* [Preprint]. https://doi.org/10.31234/osf.io/7q4m8

Kardan, O., Berman, M. G., Yourganov, G., Schmidt, J., & Henderson, J. M. (2015). Classifying mental states from eye movements during scene viewing. *Journal of Experimental Psychology. Human Perception and Performance*, *41*(6), 1502–1514. https://doi.org/10.1037/a0039673

Kardan, O., Henderson, J. M., Yourganov, G., & Berman, M. G. (2016). Observers' cognitive states modulate how visual inputs relate to gaze control. *Journal of Experimental Psychology. Human Perception and Performance*, *42*(9), 1429–1442. https://doi.org/10.1037/xhp0000224

Kardan, O., Reuter-Lorenz, P. A., Peltier, S., Churchill, N. W., Misic, B., Askren, M. K., … Berman, M. G. (2019). Brain connectivity tracks effects of chemotherapy separately from behavioral measures. *NeuroImage: Clinical*, 101654. https://doi.org/10.1016/j.nicl.2019.101654

Kardan, O., Shneidman, L., Krogh-Jespersen, S., Gaskins, S., Berman, M. G., & Woodward, A. (2017). Cultural and Developmental Influences on Overt Visual Attention to Videos. *Scientific Reports*, *7*(1), 11264. https://doi.org/10.1038/s41598-017-11570-w

Kinouchi, O., & Copelli, M. (2006). Optimal dynamical range of excitable networks at criticality. *Nature Physics*, *2*(5), 348. https://doi.org/10.1038/nphys289

Kirk, R. E. (2012). Experimental Design. In *Handbook of Psychology, Second Edition*. https://doi.org/10.1002/9781118133880.hop202001

Kitzbichler, M. G., Henson, R. N. A., Smith, M. L., Nathan, P. J., & Bullmore, E. T. (2011). Cognitive Effort Drives Workspace Configuration of Human Brain Functional Networks. *Journal of Neuroscience*, *31*(22), 8259–8270. https://doi.org/10.1523/JNEUROSCI.0440-11.2011

Kitzbichler, M. G., Smith, M. L., Christensen, S. R., & Bullmore, E. (2009). Broadband Criticality of Human Brain Network Synchronization. *PLOS Computational Biology*, *5*(3), e1000314. https://doi.org/10.1371/journal.pcbi.1000314

Latham, P. E., & Nirenberg, S. (2004). Computing and Stability in Cortical Networks. *Neural Computation*, *16*(7), 1385–1412. https://doi.org/10.1162/089976604323057434

Luck, S. J., & Vogel, E. K. (2013). Visual working memory capacity: from psychophysics and neurobiology to individual differences. *Trends in Cognitive Sciences*, *17*(8), 391–400. https://doi.org/10.1016/j.tics.2013.06.006

Mance, I. (2015). *The Contribution of Alpha Oscillations to Working Memory Processing*. Retrieved from https://scholarsbank.uoregon.edu/xmlui/handle/1794/19226

Muñoz, M. A. (2018). Colloquium: Criticality and dynamical scaling in living systems. *Reviews of Modern Physics*, *90*(3), 031001. https://doi.org/10.1103/RevModPhys.90.031001

Otto, A. R., & Daw, N. D. (2018). The opportunity cost of time modulates cognitive effort. *Neuropsychologia*. https://doi.org/10.1016/j.neuropsychologia.2018.05.006

Paas, F., Tuovinen, J. E., Tabbers, H., & Gerven, P. W. M. V. (2003). Cognitive Load Measurement as a Means to Advance Cognitive Load Theory. *Educational Psychologist*, *38*(1), 63–71. https://doi.org/10.1207/S15326985EP3801_8

Pelli, D. G. (1997). The VideoToolbox software for visual psychophysics: transforming numbers into movies. *Spatial Vision*, *10*(4), 437–442. https://doi.org/10.1163/156856897X00366

Peng, C.-K., Havlin, S., Hausdorff, J. M., Mietus, J. E., Stanley, H. E., & Goldberger, A. L. (1995). Fractal mechanisms and heart rate dynamics: Long-range correlations and their breakdown with disease. *Journal of Electrocardiology*, *28*, 59–65. https://doi.org/10.1016/S0022-0736(95)80017-4

Proekt, A., Banavar, J. R., Maritan, A., & Pfaff, D. W. (2012). Scale invariance in the dynamics of spontaneous behavior. *Proceedings of the National Academy of Sciences*, *109*(26), 10564–10569. https://doi.org/10.1073/pnas.1206894109

Rosenberg, M. D., Finn, E. S., Scheinost, D., Papademetris, X., Shen, X., Constable, R. T., & Chun, M. M. (2016). A neuromarker of sustained attention from whole-brain functional connectivity. *Nature Neuroscience*, *19*(1), 165–171. https://doi.org/10.1038/nn.4179

Rouder, J. N., Morey, R. D., Cowan, N., Zwilling, C. E., Morey, C. C., & Pratte, M. S. (2008). An assessment of fixed-capacity models of visual working memory. *Proceedings of the National Academy of Sciences*, *105*(16), 5975–5979. https://doi.org/10.1073/pnas.0711295105

Sederberg, P. B., Kahana, M. J., Howard, M. W., Donner, E. J., & Madsen, J. R. (2003). Theta and Gamma Oscillations during Encoding Predict Subsequent Recall. *Journal of Neuroscience*, *23*(34), 10809–10814. https://doi.org/10.1523/JNEUROSCI.23-34-10809.2003

Shew, W. L., & Plenz, D. (2013). The Functional Benefits of Criticality in the Cortex. *The Neuroscientist*, *19*(1), 88–100. https://doi.org/10.1177/1073858412445487

Shriki, O., Alstott, J., Carver, F., Holroyd, T., Henson, R. N. A., Smith, M. L., … Plenz, D. (2013). Neuronal Avalanches in the Resting MEG of the Human Brain. *Journal of Neuroscience*, *33*(16), 7079–7090. https://doi.org/10.1523/JNEUROSCI.4286-12.2013

Shriki, O., & Yellin, D. (2016). Optimal Information Representation and Criticality in an Adaptive Sensory Recurrent Neuronal Network. *PLOS Computational Biology*, *12*(2), e1004698. https://doi.org/10.1371/journal.pcbi.1004698

Smith, S. M., Nichols, T. E., Vidaurre, D., Winkler, A. M., Behrens, T. E. J., Glasser, M. F., … Miller, K. L. (2015). A positive-negative mode of population covariation links brain connectivity, demographics and behavior. *Nature Neuroscience*, *18*(11), 1565–1567. https://doi.org/10.1038/nn.4125

Stanislaw, H., & Todorov, N. (1999). Calculation of signal detection theory measures. *Behavior Research Methods, Instruments, & Computers*, *31*(1), 137–149. https://doi.org/10.3758/BF03207704

Tanaka, T., Kaneko, T., & Aoyagi, T. (2008). Recurrent Infomax Generates Cell Assemblies, Neuronal Avalanches, and Simple Cell-Like Selectivity. *Neural Computation*, *21*(4), 1038–1067. https://doi.org/10.1162/neco.2008.03-08-727

Van de Ville, D., Britz, J., & Michel, C. M. (2010). EEG microstate sequences in healthy humans at rest reveal scale-free dynamics. *Proceedings of the National Academy of Sciences*, 201007841. https://doi.org/10.1073/pnas.1007841107

Vogel, E. K., & Machizawa, M. G. (2004). Neural activity predicts individual differences in visual working memory capacity. *Nature*, *428*(6984), 748–751. https://doi.org/10.1038/nature02447

von Wegner, F., Laufs, H., & Tagliazucchi, E. (2018). Mutual information identifies spurious Hurst phenomena in resting state EEG and fMRI data. *Physical Review E*, *97*(2). https://doi.org/10.1103/PhysRevE.97.022415

Wendt, H., Abry, P., & Jaffard, S. (2007). Bootstrap for Empirical Multifractal Analysis. *IEEE Signal Processing Magazine*, *24*(4), 38–48. https://doi.org/10.1109/MSP.2007.4286563

Werner, G. (2010). Fractals in the nervous system: conceptual implications for theoretical neuroscience. *Frontiers in Physiology*, *1*. https://doi.org/10.3389/fphys.2010.00015

Westbrook, A., & Braver, T. S. (2015). Cognitive effort: A neuroeconomic approach. *Cognitive, Affective, & Behavioral Neuroscience*, *15*(2), 395–415. https://doi.org/10.3758/s13415-015-0334-y

Yu, S., Ribeiro, T. L., Meisel, C., Chou, S., Mitz, A., Saunders, R., & Plenz, D. (2017). Maintained avalanche dynamics during task-induced changes of neuronal activity in nonhuman primates. *ELife*, *6*, e27119. https://doi.org/10.7554/eLife.27119

## Appendix A: Supplementary materials for chapter 1

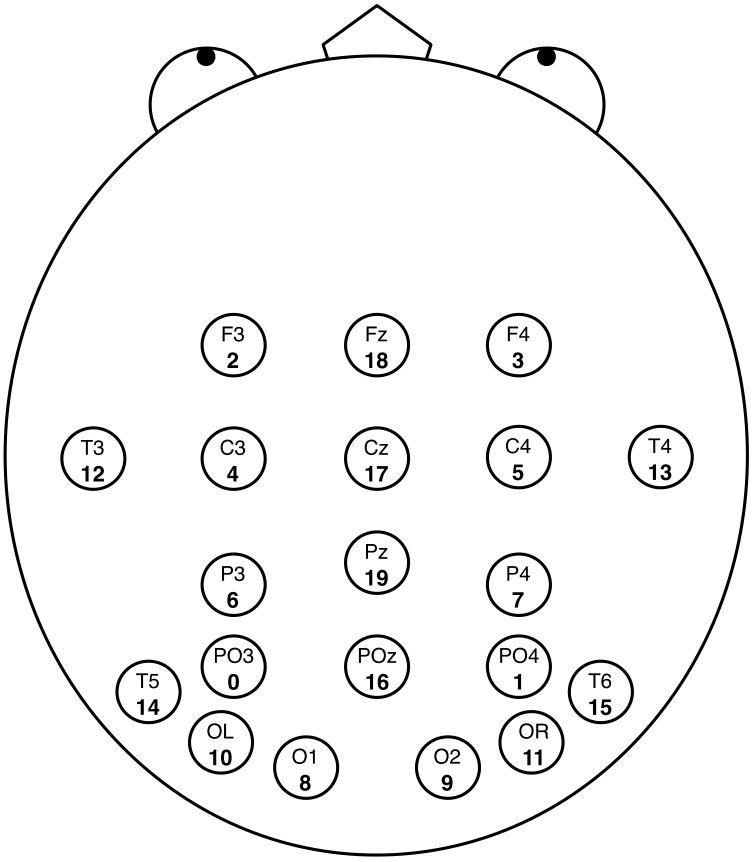


**Figure S1.1.** The electrode positions in the experiments.

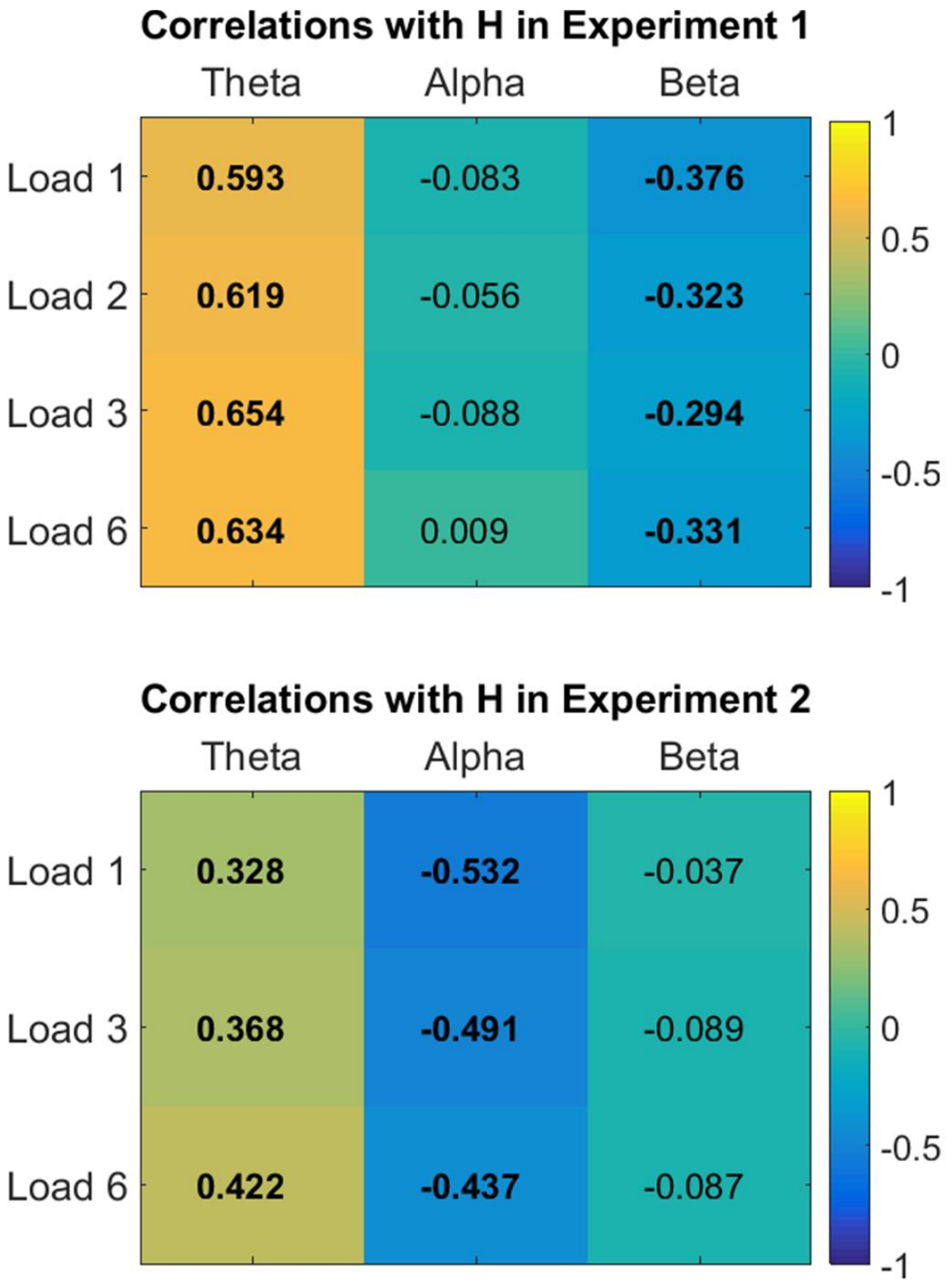


**Figure S1.2.** Correlations of theta, alpha, and beta band powers with scale-invariance (*H*) within each set size in experiments 1 and 2.

## CCA for theta and beta bands

Neither theta nor beta band powers had a stable relationship with set size in Experiment 1 (see Figure S3). In experiment 2, only theta band power showed a stable relationship with the set size (Figure S4), but this relationship could not be responsible for the pattern observed for *H* for two reasons: 1) The spatial pattern of the *H* in in experiment 2 showed a global suppression, whereas there is a more sparse and spatially heterogeneous relationship between theta power and set size (where higher set sizes correspond to less power in central and more power in occipital electrodes), and 2) The strength of the association is smaller for theta compared to *H* ( r= 0.50 vs. r = 0.65, respectively).

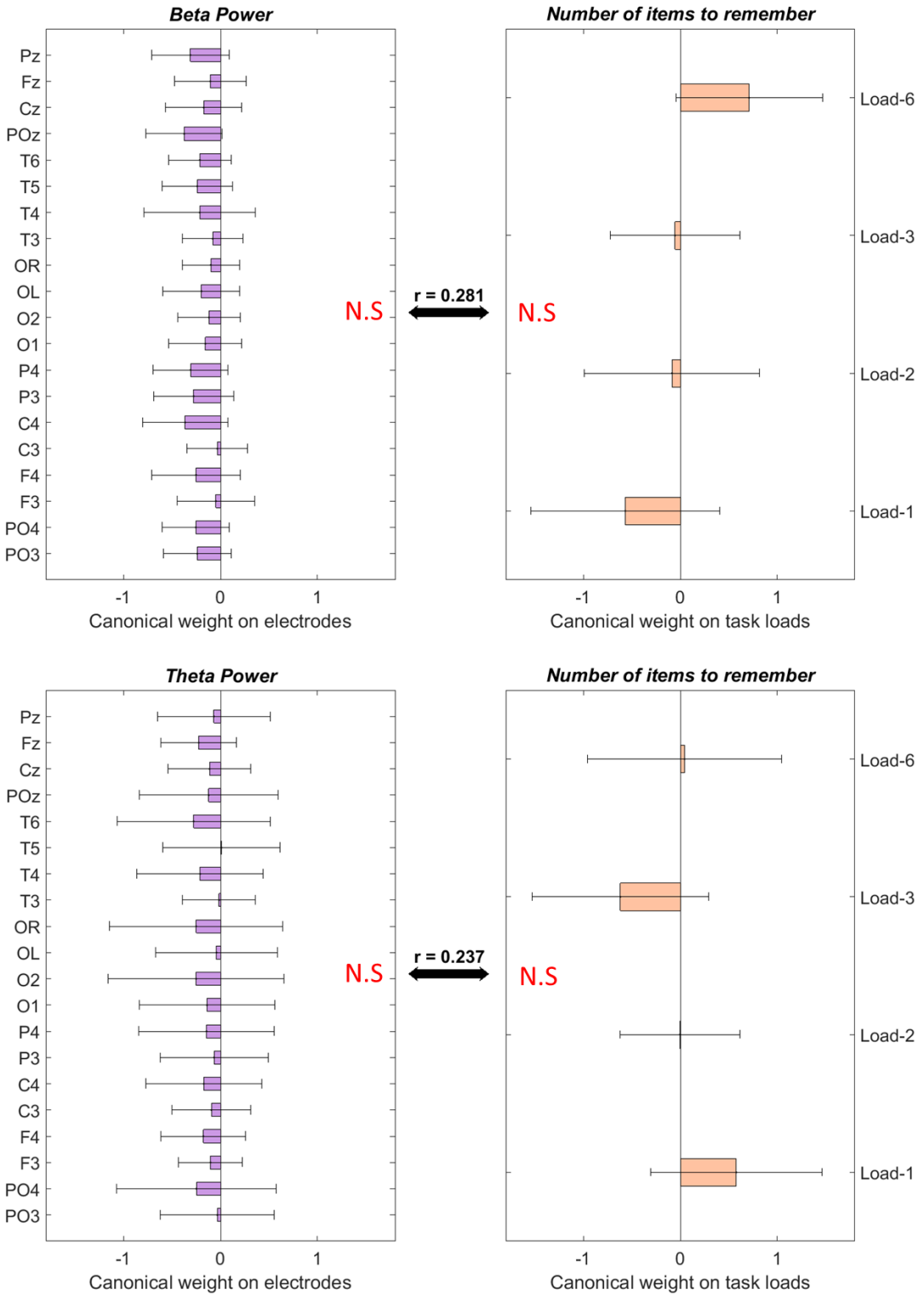


**Figure S1.3.** CCA results relating the power of theta and beta band oscillations during retention period to the task load levels in experiment 1.

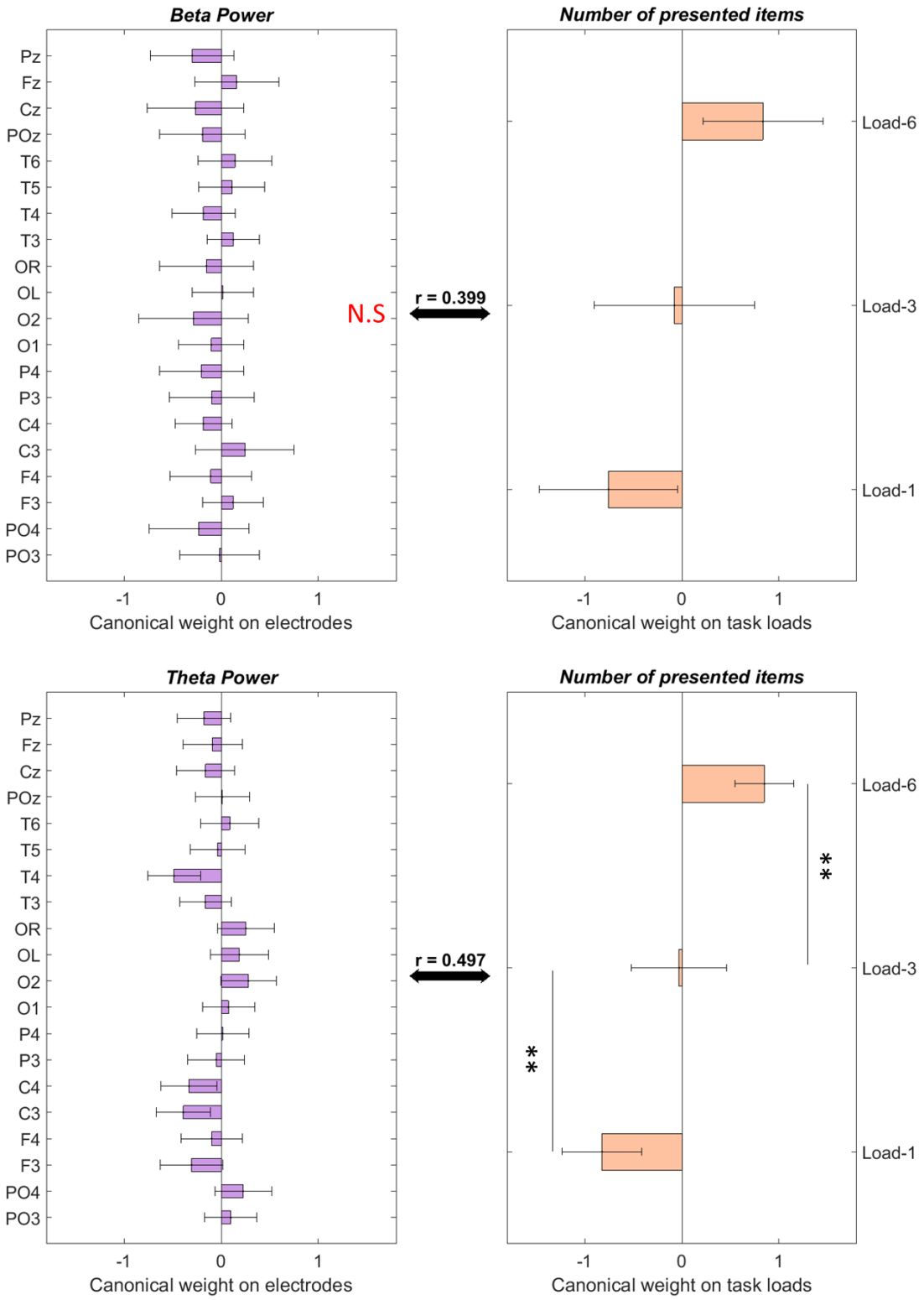


**Figure S1.4.** CCA results relating the power of theta and beta band oscillations during retention period to the task load levels in experiment 2.

## Appendix B: Supplementary material for chapter 2

**Table S2.1.** The % of the ROI voxels used for classification in each anatomically significant brain structure is listed below. The structures with less than 10 voxels overlap (i. e., < 0.2% overlap) are omitted for brevity.

| Brain Structure | % Overlap of ROI |
|---|---|
| White Matter | 57.54 |
| Left Cerebrum | 46.80 |
| Right Cerebrum | 41.46 |
| Frontal Lobe | 36.02 |
| Gray Matter | 25.43 |
| Temporal Lobe | 17.63 |
| Sub-Gyral | 17.11 |
| Sub-lobar | 15.25 |
| Middle Frontal Gyrus | 8.90 |
| Extra-Nuclear | 7.08 |
| Limbic Lobe | 6.99 |
| Parietal Lobe | 6.46 |
| Precentral Gyrus | 6.03 |
| Inferior Frontal Gyrus | 5.95 |
| Occipital Lobe | 5.77 |
| Superior Temporal Gyrus | 5.69 |
| Left Cerebellum | 5.65 |
| Middle Temporal Gyrus | 5.13 |
| Precentral_R (aal) | 4.53 |
| Cerebellum Posterior Lobe | 4.26 |
| Frontal_Mid_L (aal) | 4.13 |
| Cingulate Gyrus | 4.04 |
| Superior Frontal Gyrus | 4.00 |
| Thalamus | 3.51 |
| brodmann area 6 | 3.46 |
| Temporal_Mid_L (aal) | 3.40 |
| Middle Occipital Gyrus | 2.80 |
| Postcentral Gyrus | 2.78 |
| Cerebellar Tonsil | 2.63 |

**Table S2.1. Continued.**

| | |
|---|---|
| Thalamus_R (aal) | 2.54 |
| Temporal_Sup_R (aal) | 2.42 |
| Insula | 2.33 |
| Frontal_Mid_R (aal) | 2.29 |
| Precentral_L (aal) | 2.29 |
| Frontal_Sup_L (aal) | 2.08 |
| Frontal_Inf_Oper_R (aal) | 2.01 |
| Postcentral_L (aal) | 1.97 |
| Frontal_Inf_Tri_L (aal) | 1.95 |
| Cingulum_Mid_R (aal) | 1.93 |
| Temporal_Sup_L (aal) | 1.77 |
| Frontal_Inf_Tri_R (aal) | 1.75 |
| Occipital_Mid_L (aal) | 1.71 |
| brodmann area 9 | 1.69 |
| Medial Frontal Gyrus | 1.69 |
| Corpus Callosum | 1.65 |
| Occipital_Mid_R (aal) | 1.63 |
| brodmann area 10 | 1.62 |
| brodmann area 22 | 1.54 |
| Cerebro-Spinal Fluid | 1.54 |
| Temporal_Inf_L (aal) | 1.52 |
| Lateral Ventricle | 1.52 |
| Pulvinar | 1.52 |
| Parahippocampa Gyrus | 1.48 |
| Postcentral_R (aal) | 1.45 |
| Cerebellum Anterior Lobe | 1.39 |
| brodmann area 19 | 1.39 |
| Inferior Parietal Lobule | 1.35 |
| Fusiform_L (aal) | 1.31 |
| Anterior Cingulate | 1.22 |
| Cerebelum_Crus1_L (aal) | 1.18 |
| Rolandic_Oper_R (aal) | 1.15 |
| Cerebelum_Crus2_L (aal) | 1.13 |
| Thalamus_L (aal) | 1.11 |
| brodmann area 8 | 1.03 |
| Occipital_Inf_R (aal) | 1.01 |
| Culmen | 1.00 |
| Frontal_Sup_Medial_L (aal) | 1.00 |
| Parietal_Inf_L (aal) | 0.98 |
| Fusiform Gyrus | 0.88 |

**Table S2.1. Continued.**

| | |
|---|---|
| Cerebelum_8_L (aal) | 0.88 |
| Insula_L (aal) | 0.85 |
| brodmann area 21 | 0.83 |
| brodmann area 13 | 0.83 |
| Temporal_Mid_R (aal) | 0.77 |
| Caudate_L (aal) | 0.75 |
| Caudate | 0.71 |
| brodmann area 4 | 0.71 |
| Frontal_Inf_Orb_L (aal) | 0.69 |
| Rolandic_Oper_L (aal) | 0.69 |
| Cingulum_Ant_R (aal) | 0.69 |
| Frontal_Mid_Orb_L (aal) | 0.66 |
| brodmann area 40 | 0.64 |
| Paracentral Lobule | 0.62 |
| Inferior Semi-Lunar Lobule | 0.62 |
| SupraMarginal_L (aal) | 0.62 |
| Inferior Temporal Gyrus | 0.60 |
| Inter-Hemispheric | 0.58 |
| Lingual_L (aal) | 0.58 |
| Precuneus | 0.58 |
| Tuber | 0.58 |
| Precuneus_R (aal) | 0.56 |
| Cerebelum_9_L (aal) | 0.54 |
| brodmann area 31 | 0.54 |
| brodmann area 37 | 0.54 |
| brodmann area 3 | 0.53 |
| brodmann area 39 | 0.53 |
| Hippocampus_R (aal) | 0.51 |
| Insula_R (aal) | 0.51 |
| Cingulum_Mid_L (aal) | 0.51 |
| Caudate Body | 0.51 |
| Supp_Motor_Area_R (aal) | 0.51 |
| brodmann area 2 | 0.51 |
| brodmann area 44 | 0.49 |
| Inferior Occipital Gyrus | 0.47 |
| brodmann area 46 | 0.47 |
| Frontal_Sup_Medial_R (aal) | 0.47 |
| Cerebelum_7b_L (aal) | 0.43 |
| Frontal_Sup_R (aal) | 0.41 |

**Table S2.1. Continued.**

| | |
|---|---|
| Hippocampus_L (aal) | 0.39 |
| Medial Dorsal Nucleus | 0.39 |
| Ventral Lateral Nucleus | 0.39 |
| brodmann area 18 | 0.39 |
| brodmann area 24 | 0.38 |
| Occipital_Sup_L (aal) | 0.36 |
| Precuneus_L (aal) | 0.36 |
| ParaHippocampal_L (aal) | 0.36 |
| Temporal_Inf_R (aal) | 0.34 |
| Cuneus | 0.32 |
| Temporal_Pole_Sup_L (aal) | 0.32 |
| brodmann area 32 | 0.32 |
| brodmann area 41 | 0.32 |
| Frontal_Inf_Oper_L (aal) | 0.32 |
| Midbrain | 0.30 |
| Calcarine_L (aal) | 0.30 |
| Right Brainstem | 0.30 |
| Supramarginal Gyrus | 0.30 |
| brodmann area 45 | 0.28 |
| Cerebelum_6_L (aal) | 0.28 |
| brodmann area 20 | 0.28 |
| Pyramis | 0.26 |
| Paracentral_Lobule_R (aal) | 0.24 |
| brodmann area 42 | 0.24 |
| ParaHippocampal_R (aal) | 0.24 |
| Transverse Temporal Gyrus | 0.23 |
| brodmann area 47 | 0.23 |
| Cingulum_Post_R (aal) | 0.21 |
| Caudate Tail | 0.21 |
| brodmann area 11 | 0.21 |
| SupraMarginal_R (aal) | 0.21 |
| Putamen | 0.19 |
| Lentiform Nucleus | 0.19 |

**Table S2.2.** The % connections in the classification COI for each node (CC-400 region), together with the AAL-116 (Automated Anatomical Labeling) anatomical labels of voxels in the node are shown below. Numbers in brackets in the AAL label column shows proportion of overlap between the AAL-116 region and the CC-400 region.

| CC-400 region | % of COI | AAL label |
|---|---|---|
| **1** | 0.4602 | ["Cerebelum_4_5_L": 0.64]["Lingual_L": 0.29] |
| **2** | 0.5487 | ["Frontal_Sup_R": 0.51]["Frontal_Mid_R": 0.49] |
| **3** | 0.1770 | ["Postcentral_L": 0.94] |
| **4** | 0.4956 | ["Caudate_R": 0.96] |
| **5** | 0.1062 | ["Temporal_Sup_R": 0.85]["SupraMarginal_R": 0.15] |
| **6** | 0.0354 | ["Occipital_Mid_L": 0.77]["Temporal_Mid_L": 0.21] |
| **7** | 0.2832 | ["Frontal_Mid_L": 0.63]["Frontal_Sup_L": 0.37] |
| **8** | 0.1947 | ["Angular_R": 0.86] |
| **9** | 0.8496 | ["Insula_L": 0.74]["Frontal_Inf_Tri_L": 0.19] |
| **10** | 0.1239 | ["Rolandic_Oper_L": 0.39]["Heschl_L": 0.25]["Temporal_Sup_L": 0.25]["Insula_L": 0.12] |
| **11** | 0.0354 | ["Precuneus_L": 0.36]["Precuneus_R": 0.32]["Cingulum_Post_L": 0.18] |
| **12** | 0.0000 | ["Amygdala_R": 0.38]["Hippocampus_R": 0.36]["ParaHippocampal_R": 0.22] |
| **13** | 0.3717 | ["Cerebelum_Crus1_L": 0.88] |
| **14** | 0.5310 | ["Caudate_L": 0.98] |
| **15** | 0.6372 | ["Frontal_Mid_R": 0.75]["Frontal_Inf_Oper_R": 0.25] |
| **16** | 0.2655 | ["Frontal_Mid_R": 0.80]["Precentral_R": 0.13] |
| **17** | 0.0177 | ["Cerebelum_Crus1_R": 0.89]["Cerebelum_Crus2_R": 0.11] |
| **18** | 0.6549 | ["Cerebelum_6_L": 0.60]["Cerebelum_Crus1_L": 0.40] |
| **19** | 0.1770 | ["Temporal_Pole_Sup_L": 0.80]["Temporal_Pole_Mid_L": 0.20] |
| **20** | 0.4248 | ["Cingulum_Mid_L": 0.79]["Supp_Motor_Area_L": 0.21] |
| **21** | 0.0708 | ["Thalamus_L": 0.91] |
| **22** | 0.2124 | ["Rolandic_Oper_R": 0.55]["Insula_R": 0.40] |
| **23** | 0.0885 | ["Postcentral_R": 0.85]["Precentral_R": 0.15] |
| **24** | 0.0885 | ["Lingual_L": 0.43]["Cerebelum_Crus1_L": 0.28]["Calcarine_L": 0.14] |
| **25** | 0.0000 | ["Frontal_Inf_Orb_L": 0.59]["Frontal_Mid_Orb_L": 0.38] |
| **26** | 0.0354 | ["Temporal_Mid_R": 0.74]["Angular_R": 0.14]["Occipital_Mid_R": 0.12] |
| **27** | 0.6018 | ["Vermis_4_5": 0.26]["Vermis_6": 0.16]["Vermis_10": 0.14]["Cerebelum_4_5_L": 0.12] |
| **28** | 0.1416 | ["Paracentral_Lobule_L": 0.56]["Supp_Motor_Area_L": 0.37] |
| **29** | 0.3363 | ["Cingulum_Ant_R": 0.83]["Cingulum_Mid_R": 0.15] |
| **30** | 0.0000 | ["Temporal_Mid_L": 0.70]["Angular_L": 0.29] |
| **31** | 0.3363 | ["Frontal_Mid_Orb_R": 0.68]["Frontal_Inf_Orb_R": 0.32] |
| **32** | 0.3009 | ["Frontal_Inf_Oper_L": 0.43]["Precentral_L": 0.35]["Frontal_Mid_L": 0.12] |
| **34** | 0.1239 | ["Temporal_Inf_R": 0.38]["Temporal_Mid_R": 0.34]["Temporal_Pole_Mid_R": 0.28] |
| **35** | 0.0531 | ["Postcentral_L": 0.78]["Precentral_L": 0.21] |

**Table S2.2. Continued.**

| | | |
|---|---|---|
| **36** | **1.0088** | **["Temporal_Mid_L": 1.00]** |
| **37** | 0.1416 | ["Cuneus_R": 0.49]["Precuneus_R": 0.48] |
| **38** | 0.1770 | ["Frontal_Med_Orb_R": 0.21]["Cingulum_Ant_L": 0.19]["Frontal_Med_Orb_L": 0.14]["Cingulum_Ant_R": 0.13]["Olfactory_L": 0.11]["Olfactory_R": 0.11] |
| **39** | 0.4602 | ["Insula_L": 0.83]["Putamen_L": 0.15] |
| **40** | 1.1150 | ["Precentral_R": 0.69]["Postcentral_R": 0.31] |
| **41** | 0.2655 | ["Cerebelum_6_L": 0.60]["Cerebelum_4_5_L": 0.22] |
| **42** | 0.5841 | ["Putamen_L": 0.76]["Insula_L": 0.18] |
| **43** | 0.0000 | ["Occipital_Mid_L": 1.00] |
| **44** | 0.0000 | ["Frontal_Mid_Orb_R": 0.57]["Frontal_Sup_Orb_R": 0.43] |
| **45** | 0.1416 | ["Fusiform_L": 0.66]["Temporal_Inf_L": 0.21]["ParaHippocampal_L": 0.13] |
| **46** | 0.0708 | ["Heschl_R": 0.41]["Insula_R": 0.37]["Rolandic_Oper_R": 0.20] |
| **47** | 0.5487 | ["Cingulum_Mid_L": 0.32]["Cingulum_Mid_R": 0.26]["Cingulum_Ant_L": 0.20]["Cingulum_Ant_R": 0.18] |
| **48** | 0.0531 | ["Temporal_Inf_R": 0.85]["Temporal_Mid_R": 0.15] |
| **49** | 0.1062 | ["Parietal_Inf_L": 0.59]["SupraMarginal_L": 0.22]["Postcentral_L": 0.19] |
| **50** | 0.0531 | ["None": 1.00] |
| **51** | 0.3009 | ["Precuneus_L": 0.82]["Parietal_Sup_L": 0.18] |
| **52** | 0.1416 | ["Temporal_Mid_R": 0.59]["Temporal_Sup_R": 0.41] |
| **53** | 0.2478 | ["Frontal_Sup_Medial_L": 0.68]["Frontal_Sup_Medial_R": 0.23] |
| **54** | 0.0177 | ["Paracentral_Lobule_R": 0.71]["Paracentral_Lobule_L": 0.24] |
| **55** | 2.3363 | ["Cerebelum_6_R": 0.47]["Cerebelum_4_5_R": 0.31]["Cerebelum_10_R": 0.13] |
| **56** | 1.2212 | ["Precentral_R": 0.77]["Frontal_Inf_Oper_R": 0.20] |
| **57** | 0.1770 | ["Temporal_Mid_L": 1.00] |
| **58** | 0.3186 | ["Cuneus_L": 0.46]["Calcarine_L": 0.31]["Occipital_Sup_L": 0.13] |
| **59** | 0.0000 | ["Frontal_Sup_Medial_L": 0.42]["Frontal_Sup_L": 0.36]["Supp_Motor_Area_L": 0.21] |
| **60** | 0.2655 | ["Cingulum_Ant_R": 0.94] |
| **61** | 0.1416 | ["Parietal_Sup_R": 0.56]["Precuneus_R": 0.41] |
| **62** | 0.2124 | ["Occipital_Inf_R": 0.81]["Lingual_R": 0.12] |
| **63** | 0.0531 | ["Lingual_R": 0.49]["Calcarine_R": 0.39] |
| **64** | 0.0177 | ["Frontal_Inf_Oper_R": 0.65]["Frontal_Inf_Tri_R": 0.34] |
| **65** | 0.3717 | ["Temporal_Sup_L": 0.50]["SupraMarginal_L": 0.30]["Postcentral_L": 0.20] |
| **66** | 0.0000 | ["Temporal_Mid_L": 0.58]["Temporal_Sup_L": 0.42] |
| **67** | 0.0885 | ["Caudate_R": 0.94] |
| **68** | 0.3540 | ["SupraMarginal_R": 0.92] |
| **69** | 0.2301 | ["Temporal_Mid_R": 0.85]["Temporal_Sup_R": 0.15] |
| **70** | 0.2301 | ["Fusiform_R": 0.57]["Cerebelum_6_R": 0.32] |
| **71** | 0.2301 | ["Thalamus_R": 0.51]["None": 0.32]["Thalamus_L": 0.17] |
| **72** | 0.1416 | ["Precentral_L": 0.69]["Frontal_Mid_L": 0.17]["Frontal_Sup_L": 0.15] |
| **73** | 0.0177 | ["Parietal_Inf_L": 0.79]["Angular_L": 0.18] |
| **74** | 0.6549 | ["Frontal_Inf_Tri_L": 0.84]["Frontal_Mid_L": 0.15] |

**Table S2.2. Continued.**

| | | |
|---|---|---|
| **75** | **0.0885** | **["Insula_R": 0.51]["Frontal_Inf_Tri_R": 0.22]["Putamen_R": 0.15]["Frontal_Inf_Orb_R": 0.12]** |
| **76** | 0.1416 | ["Lingual_R": 0.84]["Cerebelum_6_R": 0.11] |
| **77** | 0.0177 | ["Cingulum_Mid_L": 0.94] |
| **78** | 0.0885 | ["Cerebelum_8_L": 0.40]["Cerebelum_Crus2_L": 0.27]["Cerebelum_Crus1_L": 0.18] |
| **80** | 0.2478 | ["Frontal_Mid_Orb_R": 0.38]["Frontal_Sup_Orb_R": 0.29]["Frontal_Sup_R": 0.25] |
| **81** | 0.5133 | ["Postcentral_R": 0.51]["Precentral_R": 0.49] |
| **82** | 0.0354 | ["Temporal_Pole_Sup_L": 0.50]["Temporal_Mid_L": 0.27] |
| **83** | 0.0177 | ["Cerebelum_Crus1_R": 0.61]["Temporal_Inf_R": 0.29] |
| **84** | 0.1416 | ["Frontal_Sup_Medial_L": 0.50]["Frontal_Sup_Medial_R": 0.39] |
| **85** | 0.0531 | ["Hippocampus_L": 0.43]["ParaHippocampal_L": 0.40]["Fusiform_L": 0.12] |
| **87** | 0.0000 | ["Fusiform_L": 0.46]["Temporal_Inf_L": 0.44] |
| **88** | 0.1593 | ["Frontal_Mid_L": 0.70]["Frontal_Inf_Tri_L": 0.30] |
| **89** | 0.0177 | ["Supp_Motor_Area_R": 0.41]["Supp_Motor_Area_L": 0.29]["Frontal_Sup_Medial_R": 0.16]["Frontal_Sup_Medial_L": 0.14] |
| **90** | 0.0885 | ["Precentral_L": 0.57]["Postcentral_L": 0.36] |
| **91** | 0.0531 | ["Amygdala_L": 0.42]["Hippocampus_L": 0.35] |
| **92** | 0.0531 | ["Calcarine_R": 0.52]["Precuneus_R": 0.30]["Cuneus_R": 0.17] |
| **93** | 0.2655 | ["Frontal_Sup_R": 0.61]["Frontal_Mid_R": 0.39] |
| **94** | 0.0885 | ["Temporal_Mid_L": 0.56]["Temporal_Inf_L": 0.37] |
| **95** | 0.1239 | ["Postcentral_L": 0.88]["Precentral_L": 0.12] |
| **96** | 0.3363 | ["Frontal_Mid_R": 0.73]["Frontal_Inf_Tri_R": 0.27] |
| **97** | 0.3186 | ["Cerebelum_9_R": 0.47]["None": 0.39]["Cerebelum_10_R": 0.11] |
| **98** | 0.6903 | ["Thalamus_R": 0.96] |
| **99** | 0.6549 | ["Cingulum_Mid_R": 0.54]["Cingulum_Mid_L": 0.25]["None": 0.21] |
| **100** | 1.0442 | ["Caudate_L": 0.36]["Olfactory_L": 0.26]["Olfactory_R": 0.18]["Caudate_R": 0.14] |
| **101** | 0.1593 | ["Temporal_Pole_Mid_R": 0.60]["Temporal_Pole_Sup_R": 0.40] |
| **102** | 0.0708 | ["Parietal_Inf_L": 0.82]["Postcentral_L": 0.15] |
| **103** | 0.4248 | ["Cingulum_Mid_R": 0.87] |
| **104** | 0.1947 | ["Parietal_Sup_L": 0.55]["Precuneus_L": 0.44] |
| **105** | 0.6018 | ["Occipital_Mid_R": 0.47]["Temporal_Mid_R": 0.44] |
| **106** | 0.1239 | ["Frontal_Sup_L": 0.69]["Frontal_Mid_L": 0.31] |
| **107** | 0.0531 | ["Putamen_R": 0.85]["Pallidum_R": 0.15] |
| **108** | 0.0531 | ["Cuneus_L": 0.83]["Occipital_Sup_L": 0.17] |
| **109** | 0.5310 | ["Cingulum_Ant_L": 0.55]["Cingulum_Ant_R": 0.45] |
| **110** | 0.4248 | ["Temporal_Inf_R": 0.90] |
| **111** | 0.0000 | ["Fusiform_R": 0.65]["ParaHippocampal_R": 0.31] |
| **112** | 0.0177 | ["Temporal_Inf_L": 0.69]["None": 0.16]["Temporal_Pole_Mid_L": 0.11] |
| **113** | 0.0177 | ["Supp_Motor_Area_R": 0.99] |
| **114** | 0.0000 | ["Occipital_Mid_L": 0.97] |
| **115** | 0.0885 | ["SupraMarginal_R": 1.00] |

**Table S2.2. Continued.**

| | | |
|---|---|---|
| **116** | **0.8142** | **["Frontal_Sup_Medial_R": 0.78]["Frontal_Sup_R": 0.22]** |
| **117** | 0.0177 | ["Postcentral_L": 0.94] |
| **118** | 0.0177 | ["Precuneus_L": 0.77]["Cingulum_Mid_L": 0.23] |
| **119** | 0.0885 | ["Cerebelum_Crus1_R": 0.92] |
| **120** | 0.0177 | ["Occipital_Mid_L": 0.90] |
| **121** | 0.0354 | ["Frontal_Inf_Orb_R": 0.77]["Frontal_Mid_Orb_R": 0.12]["Frontal_Sup_Orb_R": 0.11] |
| **122** | 0.0531 | ["Calcarine_L": 0.59]["Lingual_L": 0.39] |
| **123** | 0.4779 | ["Frontal_Inf_Orb_L": 0.78]["Frontal_Inf_Tri_L": 0.22] |
| **124** | 0.1770 | ["Postcentral_R": 0.55]["Paracentral_Lobule_R": 0.35] |
| **125** | 0.0708 | ["Putamen_R": 0.81]["Pallidum_R": 0.19] |
| **126** | 0.4956 | ["None": 1.00] |
| **127** | 0.0177 | ["Cerebelum_Crus1_L": 0.82]["Cerebelum_Crus2_L": 0.18] |
| **128** | 0.6549 | ["Temporal_Mid_R": 0.54]["Temporal_Sup_R": 0.45] |
| **129** | 0.0531 | ["Frontal_Sup_L": 0.62]["Frontal_Mid_L": 0.35] |
| **130** | 0.1062 | ["Insula_L": 0.37]["Putamen_L": 0.35]["Temporal_Sup_L": 0.15] |
| **131** | 0.1062 | ["Frontal_Inf_Tri_L": 0.93] |
| **132** | 0.1593 | ["Thalamus_L": 0.50]["None": 0.25]["Hippocampus_L": 0.20] |
| **133** | 0.1593 | ["Frontal_Inf_Tri_R": 0.82]["Frontal_Inf_Orb_R": 0.18] |
| **134** | 0.0708 | ["Cerebelum_Crus1_R": 0.85] |
| **135** | 0.0531 | ["Occipital_Mid_R": 0.67]["Angular_R": 0.33] |
| **136** | 0.3894 | ["Cerebelum_Crus2_L": 0.68]["Cerebelum_Crus1_L": 0.30] |
| **137** | 0.1593 | ["Cingulum_Post_L": 0.38]["Cingulum_Post_R": 0.25]["Cingulum_Mid_R": 0.22] |
| **138** | 0.9735 | ["Angular_L": 0.39]["Parietal_Inf_L": 0.38]["SupraMarginal_L": 0.23] |
| **139** | 0.1062 | ["Hippocampus_L": 0.50]["ParaHippocampal_L": 0.30]["Amygdala_L": 0.12] |
| **140** | 0.0885 | ["Frontal_Inf_Orb_L": 0.87]["Frontal_Mid_Orb_L": 0.13] |
| **141** | 0.0000 | ["SupraMarginal_R": 0.50]["Angular_R": 0.45] |
| **142** | 0.3717 | ["Frontal_Sup_Medial_R": 0.93] |
| **143** | 0.0531 | ["Temporal_Inf_R": 0.65]["Temporal_Pole_Mid_R": 0.31] |
| **144** | 0.4956 | ["Vermis_8": 0.48]["Cerebelum_8_R": 0.32] |
| **145** | 0.2478 | ["Precentral_L": 0.74]["Frontal_Sup_L": 0.23] |
| **146** | 0.1947 | ["Fusiform_R": 0.68]["Lingual_R": 0.16] |
| **147** | 0.2124 | ["Precentral_R": 0.58]["Frontal_Sup_R": 0.42] |
| **148** | 0.3186 | ["Insula_L": 0.78]["Frontal_Inf_Oper_L": 0.18] |
| **149** | 0.1593 | ["Rectus_L": 0.37]["Rectus_R": 0.31]["Frontal_Med_Orb_L": 0.19]["Frontal_Med_Orb_R": 0.13] |
| **150** | 0.0885 | ["Supp_Motor_Area_R": 0.50]["Frontal_Sup_R": 0.42] |
| **151** | 0.1770 | ["Cuneus_R": 0.55]["Occipital_Sup_R": 0.31]["Calcarine_R": 0.13] |
| **152** | 1.1681 | ["None": 1.00] |
| **153** | 1.3805 | ["Frontal_Mid_R": 1.00] |
| **154** | 0.0885 | ["Frontal_Sup_L": 0.70]["Frontal_Mid_L": 0.30] |
| **155** | 1.5398 | ["Temporal_Mid_R": 0.67]["Temporal_Inf_R": 0.33] |

**Table S2.2. Continued.**

| | | |
|---|---|---|
| **156** | **0.1770** | **["Cingulum_Mid_L": 0.56]["Supp_Motor_Area_L": 0.33]** |
| **157** | 0.3717 | ["Temporal_Mid_L": 0.70]["Temporal_Sup_L": 0.30] |
| **158** | 0.3540 | ["Cingulum_Ant_L": 0.54]["Frontal_Sup_Medial_L": 0.46] |
| **159** | 0.2478 | ["Precentral_R": 0.70]["Frontal_Mid_R": 0.30] |
| **160** | 0.0177 | ["Frontal_Mid_L": 0.91] |
| **161** | 0.4425 | ["Insula_L": 0.52]["Rolandic_Oper_L": 0.46] |
| **162** | 0.2655 | ["Insula_R": 0.75]["Rolandic_Oper_R": 0.13] |
| **163** | 0.2478 | ["Calcarine_R": 0.69]["Lingual_R": 0.25] |
| **164** | 0.2478 | ["Angular_L": 0.79]["Parietal_Inf_L": 0.16] |
| **165** | 0.3540 | ["Rolandic_Oper_R": 0.61]["Precentral_R": 0.23]["Postcentral_R": 0.16] |
| **166** | 0.2301 | ["Fusiform_R": 0.41]["Hippocampus_R": 0.21]["Temporal_Inf_R": 0.20]["ParaHippocampal_R": 0.18] |
| **167** | 0.6549 | ["Frontal_Sup_L": 0.70]["Frontal_Mid_L": 0.27] |
| **168** | 0.3894 | ["Caudate_L": 0.42]["Putamen_L": 0.30]["Rectus_L": 0.22] |
| **169** | 0.0354 | ["Occipital_Inf_R": 0.85] |
| **170** | 0.3894 | ["Caudate_R": 0.37]["Olfactory_R": 0.26]["Rectus_R": 0.20]["Putamen_R": 0.13] |
| **171** | 0.0000 | ["Paracentral_Lobule_L": 0.56]["Precuneus_L": 0.37] |
| **172** | 0.4602 | ["Frontal_Mid_Orb_R": 0.81]["Frontal_Mid_R": 0.19] |
| **173** | 0.0708 | ["Occipital_Inf_L": 0.89] |
| **174** | 0.1062 | ["Frontal_Sup_R": 0.81]["Supp_Motor_Area_R": 0.19] |
| **175** | 0.0354 | ["Cerebelum_6_L": 0.75]["Cerebelum_Crus1_L": 0.24] |
| **176** | 0.1416 | ["Calcarine_L": 0.79]["Occipital_Sup_L": 0.11] |
| **177** | 0.1416 | ["Calcarine_L": 0.35]["Precuneus_L": 0.28]["Lingual_L": 0.26] |
| **178** | 0.4602 | ["Frontal_Sup_Medial_L": 0.83]["Frontal_Sup_L": 0.17] |
| **179** | 0.3363 | ["Cerebelum_Crus1_R": 0.64]["Cerebelum_6_R": 0.22]["Cerebelum_Crus2_R": 0.12] |
| **180** | 0.0885 | ["Lingual_R": 0.55]["Precuneus_R": 0.17]["Vermis_4_5": 0.16] |
| **181** | 0.3894 | ["Parietal_Sup_L": 0.86]["Parietal_Inf_L": 0.14] |
| **182** | 0.0177 | ["Temporal_Inf_L": 0.32]["Fusiform_L": 0.29]["Temporal_Pole_Mid_L": 0.25] |
| **183** | 1.0619 | ["Occipital_Mid_R": 0.53]["Occipital_Sup_R": 0.47] |
| **184** | 0.7257 | ["Cingulum_Ant_L": 0.39]["Cingulum_Ant_R": 0.32]["Cingulum_Mid_L": 0.27] |
| **185** | 0.1062 | ["Thalamus_L": 0.54]["Thalamus_R": 0.46] |
| **186** | 0.2301 | ["Frontal_Mid_L": 0.80]["Precentral_L": 0.20] |
| **187** | 0.1239 | ["Precentral_L": 0.61]["Postcentral_L": 0.39] |
| **188** | 0.0177 | ["Fusiform_L": 0.80]["Cerebelum_4_5_L": 0.14] |
| **189** | 0.6726 | ["Angular_L": 0.92] |
| **190** | 0.2478 | ["Frontal_Sup_R": 0.82]["Frontal_Sup_Medial_R": 0.18] |
| **191** | 0.3363 | ["Frontal_Inf_Oper_R": 0.72]["Frontal_Inf_Tri_R": 0.13] |
| **192** | 0.2832 | ["Frontal_Mid_R": 0.51]["Frontal_Inf_Tri_R": 0.36]["Frontal_Inf_Orb_R": 0.13] |
| **193** | 0.0708 | ["Precuneus_L": 0.74]["Precuneus_R": 0.22] |

**Table S2.2. Continued.**

| | | |
|---|---|---|
| **194** | **0.7611** | **["Postcentral_R": 0.74]["Precentral_R": 0.19]** |
| **195** | 0.7257 | ["Cerebelum_6_R": 0.49]["Cerebelum_4_5_R": 0.40] |
| **196** | 0.1770 | ["None": 0.93] |
| **197** | 0.0000 | ["Temporal_Mid_L": 0.98] |
| **198** | 0.0000 | ["Frontal_Inf_Tri_L": 0.64]["Frontal_Mid_L": 0.36] |
| **199** | 0.4425 | ["Postcentral_R": 0.50]["SupraMarginal_R": 0.47] |
| **200** | 0.3186 | ["Cingulum_Mid_R": 0.65]["Precuneus_R": 0.16]["Paracentral_Lobule_R": 0.12] |
| **201** | 0.0885 | ["Frontal_Inf_Orb_R": 0.49]["Insula_R": 0.41] |
| **202** | 0.0354 | ["Frontal_Mid_Orb_L": 0.77]["Frontal_Mid_L": 0.14] |
| **203** | 0.0177 | ["Fusiform_L": 0.45]["Hippocampus_L": 0.20]["Temporal_Inf_L": 0.20]["ParaHippocampal_L": 0.15] |
| **204** | 0.2124 | ["Cerebelum_Crus2_L": 0.52]["Cerebelum_Crus1_L": 0.48] |
| **205** | 0.0177 | ["Temporal_Pole_Sup_R": 0.58]["Temporal_Pole_Mid_R": 0.36] |
| **206** | 0.2832 | ["SupraMarginal_L": 0.54]["Parietal_Inf_L": 0.46] |
| **207** | 0.3717 | ["Parietal_Inf_R": 0.63]["Angular_R": 0.37] |
| **208** | 1.1504 | ["Hippocampus_R": 0.44]["Precuneus_R": 0.27] |
| **209** | 0.4779 | ["Temporal_Mid_R": 0.93] |
| **210** | 0.5133 | ["Temporal_Sup_L": 0.44]["Rolandic_Oper_L": 0.30]["Temporal_Pole_Sup_L": 0.20] |
| **211** | 0.4956 | ["Precuneus_L": 0.44]["Cuneus_L": 0.28]["Occipital_Sup_L": 0.17]["Parietal_Sup_L": 0.11] |
| **212** | 0.2478 | ["Frontal_Mid_R": 0.96] |
| **213** | 0.1062 | ["None": 0.66]["Vermis_1_2": 0.15] |
| **214** | 0.1770 | ["Frontal_Inf_Tri_L": 0.84]["Frontal_Inf_Oper_L": 0.16] |
| **215** | 0.2478 | ["Frontal_Mid_L": 0.56]["Precentral_L": 0.44] |
| **216** | 0.0531 | ["Postcentral_R": 0.62]["Parietal_Sup_R": 0.38] |
| **217** | 0.0000 | ["Temporal_Mid_L": 0.90] |
| **218** | 0.4248 | ["Temporal_Mid_R": 1.00] |
| **219** | 0.0177 | ["Occipital_Mid_L": 1.00] |
| **220** | 0.2655 | ["Postcentral_R": 0.78]["Precentral_R": 0.22] |
| **221** | 0.4956 | ["Frontal_Inf_Orb_L": 0.80]["Temporal_Pole_Sup_L": 0.18] |
| **222** | 0.2832 | ["Frontal_Mid_R": 0.50]["Precentral_R": 0.46] |
| **223** | 0.0000 | ["Cingulum_Mid_R": 0.63]["Supp_Motor_Area_R": 0.37] |
| **224** | 0.1770 | ["Insula_R": 0.61]["Temporal_Sup_R": 0.17] |
| **225** | 0.1770 | ["Lingual_R": 0.51]["Cerebelum_Crus1_R": 0.38] |
| **226** | 0.6903 | ["Cingulum_Ant_L": 0.81]["Frontal_Sup_Medial_L": 0.18] |
| **227** | 0.5664 | ["Cerebelum_6_R": 0.89] |
| **228** | 0.1416 | ["Temporal_Mid_R": 0.69]["Temporal_Inf_R": 0.31] |
| **229** | 0.0177 | ["Occipital_Sup_R": 0.69]["Cuneus_R": 0.31] |
| **230** | 0.5841 | ["Cerebelum_9_L": 0.64]["Cerebelum_10_L": 0.36] |
| **231** | 0.1593 | ["Fusiform_L": 0.42]["Lingual_L": 0.30]["Cerebelum_6_L": 0.21] |
| **232** | 0.9558 | ["Frontal_Med_Orb_R": 0.73]["Frontal_Sup_Orb_R": 0.14]["Rectus_R": 0.13] |
| **233** | 0.1239 | ["Thalamus_L": 1.00] |

**Table S2.2. Continued.**

| | | |
|---|---|---|
| **234** | **0.1947** | **["Temporal_Mid_L": 0.50]["Occipital_Mid_L": 0.49]** |
| **235** | 0.1062 | ["Frontal_Sup_L": 0.98] |
| **236** | 0.2655 | ["Temporal_Pole_Sup_R": 0.31]["Insula_R": 0.26]["Frontal_Inf_Orb_R": 0.19] |
| **237** | 0.0531 | ["Parietal_Inf_L": 1.00] |
| **238** | 0.0354 | ["Amygdala_L": 0.37]["Putamen_L": 0.32]["Hippocampus_L": 0.16] |
| **239** | 0.4602 | ["Cingulum_Mid_R": 0.48]["Cingulum_Mid_L": 0.38]["None": 0.14] |
| **240** | 0.2832 | ["Precuneus_R": 0.71]["Parietal_Sup_R": 0.17]["Precuneus_L": 0.13] |
| **241** | 0.0000 | ["Frontal_Sup_R": 0.59]["Frontal_Mid_R": 0.38] |
| **242** | 0.2301 | ["None": 0.45]["Lingual_R": 0.22]["Thalamus_R": 0.19] |
| **243** | 0.3009 | ["Temporal_Mid_L": 0.70]["Temporal_Sup_L": 0.30] |
| **244** | 0.0885 | ["Paracentral_Lobule_L": 0.46]["Supp_Motor_Area_R": 0.17]["Cingulum_Mid_L": 0.12]["Paracentral_Lobule_R": 0.11] |
| **245** | 0.3894 | ["None": 0.51]["Thalamus_L": 0.22]["Thalamus_R": 0.16] |
| **246** | 0.2478 | ["Insula_R": 0.54]["Temporal_Sup_R": 0.21]["Putamen_R": 0.13] |
| **247** | 0.0177 | ["Cerebelum_9_L": 0.40]["None": 0.31]["Vermis_10": 0.21] |
| **248** | 0.0177 | ["Precuneus_R": 0.72]["Cingulum_Mid_R": 0.20] |
| **249** | 0.1239 | ["Frontal_Sup_L": 0.62]["Frontal_Mid_L": 0.38] |
| **250** | 0.4602 | ["Postcentral_R": 0.30]["Rolandic_Oper_R": 0.27]["Temporal_Sup_R": 0.26]["SupraMarginal_R": 0.16] |
| **251** | 0.2301 | ["Temporal_Inf_L": 0.58]["Temporal_Mid_L": 0.42] |
| **252** | 0.4071 | ["Angular_R": 0.96] |
| **253** | 0.2832 | ["Vermis_6": 0.40]["Cerebelum_6_L": 0.37] |
| **254** | 0.1239 | ["Frontal_Sup_L": 0.41]["Frontal_Sup_Orb_L": 0.33]["Frontal_Mid_Orb_L": 0.24] |
| **255** | 0.0000 | ["Frontal_Sup_Medial_R": 0.66]["Frontal_Sup_R": 0.32] |
| **256** | 0.3363 | ["Cingulum_Mid_R": 0.89] |
| **257** | 0.0708 | ["Postcentral_L": 0.79]["Parietal_Sup_L": 0.21] |
| **258** | 0.6195 | ["Cerebelum_6_R": 0.75]["Cerebelum_Crus1_R": 0.12]["Cerebelum_8_R": 0.11] |
| **259** | 0.0708 | ["Temporal_Inf_R": 0.84] |
| **260** | 0.3009 | ["Frontal_Inf_Orb_L": 0.63]["Insula_L": 0.18] |
| **261** | 0.2655 | ["SupraMarginal_L": 0.81]["Postcentral_L": 0.19] |
| **262** | 0.0885 | ["ParaHippocampal_L": 0.57]["Cerebelum_4_5_L": 0.35] |
| **263** | 0.0708 | ["Occipital_Mid_L": 0.47]["Occipital_Sup_L": 0.39] |
| **264** | 0.3009 | ["Frontal_Med_Orb_L": 0.83]["Rectus_L": 0.15] |
| **265** | 0.6903 | ["Frontal_Inf_Tri_R": 0.93] |
| **266** | 0.0708 | ["Frontal_Mid_L": 1.00] |
| **267** | 0.7080 | ["Cerebelum_3_R": 0.53]["Cerebelum_4_5_R": 0.19]["ParaHippocampal_R": 0.13] |
| **268** | 0.1239 | ["Thalamus_L": 0.47]["Hippocampus_L": 0.25]["Lingual_L": 0.18] |
| **269** | 0.1416 | ["Cuneus_R": 0.78]["Cuneus_L": 0.18] |
| **270** | 0.3009 | ["Temporal_Sup_R": 1.00] |
| **271** | 0.5133 | ["Temporal_Pole_Sup_L": 0.56]["Temporal_Sup_L": 0.30]["Temporal_Mid_L": 0.15] |
| **272** | 0.4248 | ["Parietal_Inf_R": 0.59]["SupraMarginal_R": 0.41] |

**Table S2.2. Continued.**

| | | |
|---|---|---|
| **273** | **0.0531** | **["Frontal_Inf_Orb_R": 0.99]** |
| **274** | 0.0885 | ["Insula_L": 0.54]["Rolandic_Oper_L": 0.44] |
| **275** | 0.5841 | ["Precuneus_R": 0.86]["Precuneus_L": 0.14] |
| **276** | 0.1239 | ["Cerebelum_4_5_L": 0.66]["Cerebelum_3_L": 0.19]["None": 0.14] |
| **277** | 0.2478 | ["Temporal_Inf_R": 0.65]["Fusiform_R": 0.35] |
| **278** | 0.0354 | ["Fusiform_L": 0.35]["Temporal_Inf_L": 0.23]["Cerebelum_6_L": 0.19]["Occipital_Inf_L": 0.16] |
| **279** | 0.1416 | ["Frontal_Mid_L": 0.88] |
| **280** | 0.1062 | ["Temporal_Mid_L": 0.96] |
| **281** | 0.2301 | ["Precentral_R": 0.87]["Frontal_Sup_R": 0.11] |
| **282** | 0.0000 | ["Fusiform_L": 0.47]["Lingual_L": 0.45] |
| **283** | 1.1858 | ["Cingulum_Ant_L": 0.68]["Frontal_Med_Orb_L": 0.27] |
| **284** | 0.1416 | ["Hippocampus_R": 0.58]["ParaHippocampal_R": 0.35] |
| **285** | 0.1239 | ["Frontal_Mid_R": 1.00] |
| **286** | 0.1947 | ["Calcarine_L": 0.35]["Vermis_6": 0.16] |
| **287** | 0.1062 | ["Parietal_Sup_R": 0.75]["Parietal_Inf_R": 0.13] |
| **288** | 0.0177 | ["Temporal_Pole_Sup_R": 0.72]["Insula_R": 0.15] |
| **289** | 0.8319 | ["Frontal_Sup_Medial_R": 0.82]["Frontal_Sup_R": 0.18] |
| **290** | 0.0885 | ["Temporal_Inf_R": 0.62]["Temporal_Mid_R": 0.38] |
| **291** | 0.2832 | ["Supp_Motor_Area_L": 0.61]["Supp_Motor_Area_R": 0.39] |
| **292** | 0.3540 | ["Putamen_L": 0.27]["Pallidum_L": 0.22]["None": 0.11] |
| **293** | 0.4425 | ["Precentral_L": 0.74]["Frontal_Inf_Oper_L": 0.26] |
| **294** | 0.6903 | ["Occipital_Mid_R": 0.68]["Temporal_Mid_R": 0.32] |
| **295** | 0.3186 | ["Vermis_4_5": 0.54]["Cerebelum_4_5_R": 0.26]["Cerebelum_4_5_L": 0.14] |
| **296** | 0.0000 | ["Fusiform_L": 0.53]["Temporal_Inf_L": 0.39] |
| **297** | 0.0177 | ["Frontal_Sup_Medial_L": 0.89]["Frontal_Sup_L": 0.11] |
| **298** | 0.0531 | ["Temporal_Pole_Sup_L": 0.72]["Insula_L": 0.12] |
| **299** | 0.0531 | ["Hippocampus_R": 0.63]["ParaHippocampal_R": 0.24] |
| **300** | 0.2124 | ["Vermis_3": 0.37]["Vermis_1_2": 0.23]["Cerebelum_3_R": 0.20] |
| **301** | 0.0885 | ["Cerebelum_Crus2_L": 0.52]["Cerebelum_Crus1_L": 0.46] |
| **302** | 0.5487 | ["Temporal_Sup_R": 0.55]["SupraMarginal_R": 0.27]["Rolandic_Oper_R": 0.18] |
| **303** | 0.4248 | ["Cingulum_Mid_L": 0.67]["Supp_Motor_Area_L": 0.33] |
| **304** | 0.1416 | ["Precentral_R": 0.44]["Frontal_Mid_R": 0.29]["Frontal_Sup_R": 0.26] |
| **305** | 0.4779 | ["Temporal_Sup_L": 0.39]["Rolandic_Oper_L": 0.33]["Postcentral_L": 0.18] |
| **306** | 0.0354 | ["Frontal_Sup_R": 0.53]["Frontal_Mid_R": 0.47] |
| **307** | 0.0531 | ["Insula_R": 0.68]["Putamen_R": 0.24] |
| **308** | 0.1947 | ["Occipital_Mid_R": 0.53]["Occipital_Sup_R": 0.47] |
| **309** | 0.1416 | ["ParaHippocampal_R": 0.46]["Hippocampus_R": 0.39]["None": 0.15] |
| **310** | 0.6726 | ["None": 0.40]["Cerebelum_4_5_R": 0.38]["Cerebelum_3_R": 0.19] |
| **312** | 0.1062 | ["Temporal_Inf_L": 0.93] |

**Table S2.2. Continued.**

| | | |
|---|---|---|
| **313** | **0.0000** | **["Temporal_Pole_Mid_R": 0.52]["ParaHippocampal_R": 0.19]["Fusiform_R": 0.15]["Temporal_Inf_R": 0.13]** |
| **314** | 0.1062 | ["SupraMarginal_L": 0.60]["Temporal_Sup_L": 0.30] |
| **315** | 0.1770 | ["Cerebelum_9_L": 0.63]["Cerebelum_8_L": 0.21]["Vermis_9": 0.12] |
| **316** | 0.1239 | ["Supp_Motor_Area_L": 0.99] |
| **317** | 0.0708 | ["Rolandic_Oper_R": 0.48]["Temporal_Sup_R": 0.35]["Heschl_R": 0.17] |
| **318** | 0.0177 | ["Occipital_Inf_L": 0.35]["Cerebelum_Crus1_L": 0.34]["Lingual_L": 0.23] |
| **319** | 0.1062 | ["Temporal_Mid_L": 0.96] |
| **320** | 0.0000 | ["Frontal_Inf_Tri_R": 0.56]["Frontal_Mid_R": 0.44] |
| **321** | 0.1593 | ["Vermis_7": 0.38]["Cerebelum_Crus2_R": 0.27]["Cerebelum_Crus1_R": 0.18] |
| **322** | 0.1770 | ["Fusiform_R": 0.64]["Cerebelum_6_R": 0.28] |
| **323** | 0.3540 | ["Parietal_Inf_R": 0.45]["Parietal_Sup_R": 0.32]["Postcentral_R": 0.21] |
| **324** | 0.5487 | ["Calcarine_R": 0.53]["Calcarine_L": 0.35] |
| **325** | 0.3894 | ["Frontal_Med_Orb_R": 0.39]["Cingulum_Ant_R": 0.38]["Frontal_Sup_Medial_R": 0.22] |
| **326** | 0.2655 | ["Occipital_Sup_L": 0.71]["Occipital_Mid_L": 0.26] |
| **327** | 0.2832 | ["Precuneus_R": 0.62]["Cuneus_R": 0.25] |
| **328** | 0.2124 | ["None": 0.32]["Hippocampus_R": 0.23]["ParaHippocampal_R": 0.18]["Amygdala_R": 0.12]["Pallidum_R": 0.12] |
| **329** | 0.5133 | ["Temporal_Sup_R": 0.37]["Temporal_Mid_R": 0.33]["Temporal_Pole_Sup_R": 0.25] |
| **330** | 0.0000 | ["Fusiform_R": 0.63]["ParaHippocampal_R": 0.25] |
| **331** | 0.9027 | ["Temporal_Sup_L": 0.63]["Rolandic_Oper_L": 0.13]["Heschl_L": 0.12] |
| **332** | 0.0885 | ["Lingual_L": 0.59]["Cerebelum_6_L": 0.29] |
| **333** | 0.1239 | ["ParaHippocampal_R": 0.49]["None": 0.33]["Hippocampus_R": 0.18] |
| **334** | 0.0531 | ["Frontal_Sup_L": 0.67]["Supp_Motor_Area_L": 0.30] |
| **335** | 0.4602 | ["Cerebelum_Crus1_R": 0.76] |
| **336** | 0.0354 | ["Temporal_Sup_R": 0.54]["Rolandic_Oper_R": 0.33]["Temporal_Pole_Sup_R": 0.11] |
| **337** | 0.0000 | ["Hippocampus_L": 0.70]["ParaHippocampal_L": 0.22] |
| **338** | 0.0531 | ["Frontal_Inf_Orb_R": 0.81]["Temporal_Pole_Sup_R": 0.13] |
| **339** | 0.6372 | ["Putamen_L": 0.83]["Pallidum_L": 0.17] |
| **340** | 0.0000 | ["Occipital_Sup_L": 0.56]["Occipital_Mid_L": 0.29]["Cuneus_L": 0.15] |
| **341** | 0.1593 | ["Temporal_Mid_R": 0.46]["Temporal_Sup_R": 0.30]["Angular_R": 0.16] |
| **342** | 0.0177 | ["Calcarine_R": 0.30]["Calcarine_L": 0.23]["Cuneus_R": 0.16]["Cuneus_L": 0.13]["Precuneus_R": 0.12] |
| **343** | 1.0796 | ["Temporal_Mid_L": 0.67]["Temporal_Pole_Mid_L": 0.18]["Temporal_Inf_L": 0.13] |
| **344** | 0.1593 | ["Postcentral_R": 0.45]["SupraMarginal_R": 0.34]["Parietal_Inf_R": 0.16] |
| **345** | 0.3894 | ["Precentral_L": 0.94] |
| **346** | 0.0708 | ["Temporal_Inf_L": 0.40]["Cerebelum_Crus1_L": 0.36]["Fusiform_L": 0.14] |
| **347** | 0.0531 | ["Insula_R": 0.57]["Putamen_R": 0.19]["Frontal_Inf_Oper_R": 0.16] |
| **348** | 0.0885 | ["Calcarine_R": 0.52]["Lingual_R": 0.40] |
| **349** | 0.2478 | ["Cerebelum_9_R": 0.66]["Vermis_9": 0.26] |
| **350** | 0.0708 | ["Cerebelum_4_5_L": 0.30]["Cerebelum_3_L": 0.24]["None": 0.20]["ParaHippocampal_L": 0.14] |
| **351** | 0.3540 | ["Lingual_L": 0.48]["Calcarine_L": 0.46] |

**Table S2.2. Continued.**

| | | |
|---|---|---|
| **352** | **0.0708** | **["Supp_Motor_Area_L": 0.58]["Supp_Motor_Area_R": 0.34]** |
| **353** | 0.0531 | ["Calcarine_L": 0.51]["Cuneus_L": 0.44] |
| **354** | 0.4071 | ["Frontal_Inf_Oper_R": 0.49]["Frontal_Inf_Tri_R": 0.27]["Frontal_Mid_R": 0.14] |
| **355** | 0.1593 | ["Precuneus_L": 0.67]["Precuneus_R": 0.33] |
| **356** | 0.2124 | ["Parietal_Inf_R": 0.66]["Angular_R": 0.33] |
| **357** | 0.5310 | ["Cerebelum_Crus2_R": 0.59]["Cerebelum_Crus1_R": 0.41] |
| **359** | 0.0177 | ["Precentral_R": 0.50]["Postcentral_R": 0.50] |
| **360** | 0.1947 | ["Parietal_Inf_L": 0.44]["Parietal_Sup_L": 0.30]["Postcentral_L": 0.26] |
| **361** | 0.6195 | ["Fusiform_R": 0.70]["Cerebelum_4_5_R": 0.21] |
| **362** | 0.0000 | ["Occipital_Inf_L": 0.74]["Occipital_Mid_L": 0.25] |
| **363** | 0.0531 | ["Temporal_Sup_L": 0.73]["SupraMarginal_L": 0.24] |
| **364** | 0.4602 | ["Temporal_Mid_R": 0.87]["Temporal_Sup_R": 0.13] |
| **365** | 0.1416 | ["Caudate_R": 0.84]["Thalamus_R": 0.13] |
| **366** | 0.1947 | ["Temporal_Pole_Sup_L": 0.30]["Insula_L": 0.29]["Frontal_Inf_Orb_L": 0.25] |
| **367** | 0.1947 | ["Occipital_Mid_R": 1.00] |
| **368** | 0.0354 | ["Precuneus_L": 0.49]["Cingulum_Mid_L": 0.29]["Cingulum_Post_L": 0.22] |
| **370** | 0.1062 | ["Frontal_Inf_Oper_L": 0.71]["Rolandic_Oper_L": 0.14]["Precentral_L": 0.12] |
| **371** | 0.0354 | ["Frontal_Sup_Medial_L": 0.59]["Frontal_Sup_Medial_R": 0.24]["Cingulum_Mid_R": 0.12] |
| **372** | 0.4602 | ["Fusiform_R": 0.48]["Lingual_R": 0.30]["Cerebelum_6_R": 0.17] |
| **373** | 0.2478 | ["Caudate_L": 0.79]["Putamen_L": 0.15] |
| **374** | 0.1416 | ["Temporal_Mid_L": 0.76]["Temporal_Inf_L": 0.24] |
| **375** | 0.0000 | ["Putamen_R": 0.43]["Amygdala_R": 0.30]["Pallidum_R": 0.24] |
| **376** | 0.0885 | ["Parietal_Sup_R": 0.62]["Occipital_Sup_R": 0.17]["Precuneus_R": 0.13] |
| **377** | 0.1062 | ["Cerebelum_6_L": 0.60]["Cerebelum_4_5_L": 0.38] |
| **378** | 0.4956 | ["Lingual_R": 0.32]["Lingual_L": 0.27]["Vermis_4_5": 0.23] |
| **379** | 0.0354 | ["Frontal_Mid_L": 0.95] |
| **380** | 0.1062 | ["Cingulum_Mid_R": 0.82]["Supp_Motor_Area_R": 0.18] |
| **381** | 0.2832 | ["Parietal_Sup_L": 0.82]["Parietal_Inf_L": 0.18] |
| **383** | 0.4602 | ["Temporal_Mid_R": 0.64]["Temporal_Sup_R": 0.36] |
| **384** | 0.0000 | ["Cerebelum_Crus1_L": 0.91] |
| **385** | 0.0177 | ["Frontal_Mid_Orb_L": 0.80]["Frontal_Inf_Orb_L": 0.12] |
| **386** | 0.3363 | ["Frontal_Sup_R": 0.56]["Frontal_Mid_R": 0.44] |
| **387** | 0.0531 | ["Frontal_Mid_R": 0.85]["Frontal_Sup_R": 0.15] |
| **388** | 0.0177 | ["Temporal_Pole_Mid_L": 0.73]["Temporal_Inf_L": 0.18] |
| **389** | 0.1947 | ["Paracentral_Lobule_R": 0.44]["Precuneus_L": 0.18]["Precuneus_R": 0.15] |
| **391** | 0.2478 | ["Cerebelum_4_5_R": 0.52]["Lingual_R": 0.17]["ParaHippocampal_R": 0.15]["Cerebelum_3_R": 0.13] |
| **392** | 0.5841 | ["Frontal_Sup_Medial_L": 0.81]["Frontal_Sup_L": 0.19] |
| **393** | 0.0177 | ["Supp_Motor_Area_R": 0.81] |
| **394** | 0.0177 | ["Temporal_Sup_L": 0.68]["Insula_L": 0.32] |
| **395** | 0.0708 | ["Temporal_Mid_R": 0.76]["Temporal_Sup_R": 0.14] |

**Table S2.2. Continued.**

| | | |
|---|---|---|
| **396** | **0.0177** | **["Olfactory_R": 0.23]["Temporal_Pole_Sup_R": 0.23]["ParaHippocampal_R": 0.18]["Putamen_R": 0.11]** |
| **397** | 0.3717 | ["Frontal_Mid_R": 1.00] |
| **398** | 0.2478 | ["Thalamus_R": 0.98] |
| **399** | 0.2655 | ["None": 1.00] |
| **400** | 0.3717 | ["Frontal_Mid_L": 0.88]["Frontal_Sup_L": 0.12] |